A CONTINUOUS OXIDIZER REGRESSION MODEL
FOR THE COMBUSTION OF COMPOSITE SOLID PROPELLANTS

DTIC FILE_COPY

by Joseph John Cor
Capt, USAF

University of Illinois, 1986
Master of Science, Mechanical Engineering
109 pages

Over the past several decades, there has been a considerable effort to model the processes occurring during the combustion of composite solid propellants. Accurate models able to predict the burning rate characteristics of solid propellants would be very valuable, as they would facilitate the design of solid rocket fuels by reducing the need for laboratory testing of different solid mixtures until a mixture with the right ballistic properties is found. Using a reliable analytical model, a propellant designer could, in theory, simply input key properties of a possible propellant formulation into the model, and the model would provide an accurate prediction of what the burning rate characteristics for that mixture would be.

Earlier attempts at modeling the steady-state burning of composite solid propellants are reviewed, with an emphasis placed on the Beckstead, Derr, and Price (BDP) and Petite Ensemble Model (PEM). The Continuous Oxidizer Regression (COR) model is then described, which is a modification to the PEM model. The COR model's predictions for burning rate and pressure exponent are then compared to those of an actual solid composite propellant. The model predicts the general trends found in actual experimental data, but the model's output is found to be highly sensitive to the assumptions regarding surface geometry and flame formation, which are as yet not clearly known.

DTIC
ELECTE
OCT 2 7 1987
S D
H

87 10 14 249

REPORT DOCUMENTATION PAGE		READ INSTRUCTIONS BEFORE COMPLETING FORM
1. REPORT NUMBER AFIT/CI/NR 87-69T	2. GOVT ACCESSION NO. ADA 186742	3. RECIPIENT'S CATALOG NUMBER
4. TITLE (and Subtitle) A Continuous Oxidizer Regression Model, For The Combustion Of Composite Solid Propellants		5. TYPE OF REPORT & PERIOD COVERED THESIS/DISSERTATION
		6. PERFORMING ORG. REPORT NUMBER
7. AUTHOR(s) Joseph John Cor		8. CONTRACT OR GRANT NUMBER(s)
9. PERFORMING ORGANIZATION NAME AND ADDRESS AFIT STUDENT AT: University of Illinois		10. PROGRAM ELEMENT, PROJECT, TASK AREA & WORK UNIT NUMBERS
11. CONTROLLING OFFICE NAME AND ADDRESS AFIT/NR WPAFB OH 45433-6583		12. REPORT DATE 1986
		13. NUMBER OF PAGES 109
14. MONITORING AGENCY NAME & ADDRESS(if different from Controlling Office)		15. SECURITY CLASS. (of this report) UNCLASSIFIED
		15a. DECLASSIFICATION/DOWNGRADING SCHEDULE

16. DISTRIBUTION STATEMENT (of this Report)

APPROVED FOR PUBLIC RELEASE; DISTRIBUTION UNLIMITED

17. DISTRIBUTION STATEMENT (of the abstract entered in Block 20, if different from Report)

18. SUPPLEMENTARY NOTES
APPROVED FOR PUBLIC RELEASE: IAW AFR 190-1

LYNN E. WOLAVER May 87
Dean for Research and
Professional Development
AFIT/NR

19. KEY WORDS (Continue on reverse side if necessary and identify by block number)

20. ABSTRACT (Continue on reverse side if necessary and identify by block number)
ATTACHED

DD FORM 1473 EDITION OF 1 NOV 65 IS OBSOLETE
1 JAN 73

87   249

BIBLIOGRAPHY

1. Summerfield, M., Sutherland, G.S., Webb, M.J., Taback, H.J., and Hall, K.P., "Burning Mechanism of Ammonium Perchlorate Propellants," *ARS Progress in Astronautics and Rocketry - Vol. 1: Solid Propellant Rocket Research*, Academic Press, New York, 1960, pp. 141-182.

2. Ramohalli, K.N.R., "Steady-State Burning of Composite Propellants under Zero Cross-Flow Situation," *Fundamentals of Solid-Propellant Combustion - Progress in Astronautics and Aeronautics: Volume 90*, Edited by K. Kuo and M. Summerfield, 1984, pp. 409-477.

3. Hermance, C.E., "A Model of Composite Propellant Combustion Including Surface Heterogeneity and Heat Generation," *AIAA Journal*, Vol. 4, No. 9, September 1966, pp. 1629-1637.

4. Beckstead, M.W., Derr, R.L., and Price, C.F., "A Model of Composite Solid Propellant Combustion Based on Multiple Flames," *AIAA Journal*, Vol. 8, No. 12, December 1970, pp. 2200-2207.

5. Burke, S.P. and Schumann, T.E.W., "Diffusion Flames," *Industrial and Engineering Chemistry*, Vol. 20, No. 10, October 1928, pp. 998-1004.

6. Renie, J.P., "Combustion Modeling of Composite Solid Propellants," PhD. Thesis, Purdue University, West Lafayette, Indiana, December 1982.

7. Glick, R.L., "On Statistical Analysis of Composite Solid Propellant Combustion," *AIAA Journal*, Vol. 12, No. 3, March 1974, pp. 384-385, also "Composite Propellant Combustion Modeling," unpublished work.

8. King, M.K., "Model for Steady State Combustion of Unimodal Composite Solid Propellants," AIAA Paper No. 78-216, AIAA 16th Aerospace Sciences Meeting, Huntsville, Alabama, January 1978.

9. King, M.K., "A Model of the Effects of Pressure and Crossflow Velocity on Composite Propellant Burning Rate," AIAA Paper No. 79-1171, AIAA/SAE/ASME 15th Joint Propulsion Conference, Las Vegas, Nevada, June 1979.

10. Miller, R.R., Donohue, M.T., Yount, R.A., and Martin, J.R., "Control of Solids Distribution in HTPB Propellants," AFRPL-TR-78-14, April 1978.

11. Gordon, S. and McBride, B.J., "Computer Program for Calculation of Complex Chemical Equilibrium Compositions, Rocket Performance, Incident and Reflected Shocks, and Chapman-Jouquet Detonation," NASA-SP-273, 1971.

12. Cohen, N.S., Fleming, R.W., and Derr, R.L., "Role of Binders in Solid Propellant Combustion," *AIAA Journal*, Vol. 12, No. 2, February 1974, pp. 212-218.

13. Price, C.F., Boggs, T.L., and Derr, R.L., "The Steady-State Combustion Behavior of Ammonium Perchlorate and HMX," AIAA Paper No. 79-0164, 17th Aerospace Sciences Meeting, New Orleans, Louisiana, January 1979.

A CONTINUOUS OXIDIZER REGRESSION MODEL
FOR THE COMBUSTION OF COMPOSITE SOLID PROPELLANTS

BY

JOSEPH JOHN COR

B.S., University of Wyoming, 1982

THESIS

Submitted in partial fulfillment of the requirements
for the degree of Master of Science in Mechanical Engineering
in the Graduate College of the
University of Illinois at Urbana-Champaign, 1987

Urbana, Illinois

TABLE OF CONTENTS

LIST OF TABLES

LIST OF FIGURES

NOMENCLATURE

a	GDF Model burning rate coefficient.
a	oxidizer surface radius.
a_1, a_2, a_3	constants used in Hermance's analysis.
A	pre-exponential frequency factor.
b	constant used in Hermance's analysis.
b	fuel surface radius.
b	GDF Model burning rate coefficient.
b_1, b_2, b_3	constants used in Hermance's analysis.
c	constant in St. Roberts expression.
c, c_3	constants used in Hermance's analysis.
c_1, c_2, c_3	constants in general cubic equation.
c_p	specific heat.
C	constant used in Hermance's analysis.
d	constant used in Hermance's analysis.
d	surface diameter.
D_{ox}	oxidizer particle diameter.
D_{ox}'	pseudo-propellant oxidizer diameter at burning propellant surface.
ΔD	number of discrete particle diameters in Hermance's model.
e	annulus of fuel surrounding oxidizer particle.
E	activation energy.
h_f	height above or below the initial unburned surface at which planar fuel surface lies.
h_{ox}	height of center of oxidizer surface above or below planar fuel surface.
k	number of equal volumes per hemisphere used in the COR model's calculation of propellant burning rate.

K	constant used in Hermance's analysis.
L	diffusion flame height in GDF Model.
m	constant used in Hermance's analysis.
m	mass flux.
n	burning rate exponent.
n	constant used in Hermance's analysis.
p	pressure.
Q	flame heat release term.
Q	solution parameter for general cubic equation.
Q_L	heat of gasification for oxidizer.
Q_{fuel}	heat of pyrolysis for fuel binder.
r	linear propellant burning rate.
r	radius.
R	solution parameter for general cubic equation.
R	universal gas constant.
S	surface area.
t	time.
t_{ign}	ignition delay time for oxidizer particle.
T	temperature.
T_o	initial solid propellant temperature.
V	constant used in Hermance's analysis.
V', V''	parameters used in geometric analysis in COR model.
x	flame standoff height.
x	vertical coordinate above surface.
z	variable in general cubic equation.

Greek Symbols

α	oxidizer mass fraction.
β	dimensionless fuel annulus.
β	constant used in Hermance's analyis.
β_F	fraction of reactants entering primary flame.
δ	chemical reaction rate order.
δ	pressure exponent in Hermance's analysis.
δ	dimensionless planar oxidizer surface area.
δ'	dimensionless planar fuel surface area.
δ_{ox}	height of center of oxidizer surface below initial unburned planar surface.
ϵ	fraction of diffusion flame height at which a flat flame will produce the same heat flux back to the surface.
ϵ	fissure depth between oxidizer and fuel in Hermance's model.
ϵ	fraction of maximum diffusion flame height at which a planar sheet flame will achieve the same heat transfer back to the surface as diffusion flame.
γ	dimensionless total planar surface area.
η	oxidizer radius normalized by fuel radius.
λ	thermal conductivity.
ρ	density.
σ	dimensionless planar fuel surface area.
σ	oxidizer mode standard deviation.
θ	dimensionless temperature in Hermance's analysis.
θ	solution parameter in general cubic equation.

ξ	dimensionless height below original fuel/oxidizer surface.
ξ	dimensionless flame height.
ξ*	maximum dimensionless diffusion flame height.
ζ	volume fraction.

Superscripts

P	planar surface area quantity.
T	total surface area quantity.

Subscripts

AP	oxidizer (AP) monopropellant flame.
ave	average.
d	pseudo-propellant property.
f	fuel.
F	flame.
FD	final diffusion flame.
FF	final diffusion flame.
g	gases.
ox	oxidizer.
p	propellant.
P	planar.
PD	primary diffusion flame.
PF	primary kinetic flame.
s	surface.
sr	surface-fuel reaction area in Hermance's model.

T	total quantity for the overall propellant.
+	upper oxidizer hemisphere cut.
-	lower oxidizer hemisphere cut.

CHAPTER 1 - INTRODUCTION

Over the past several decades, there has been a considerable effort to model the processes occurring during the combustion of composite solid propellants. Accurate models able to predict the burning rate characteristics of solid propellants would be very valuable, as they would facilitate the design of solid rocket fuels by reducing the need for laboratory testing of different solid mixtures until a mixture with the right ballistic properties is found. Using a reliable analytical model, a propellant designer could, in theory, simply input key properties of a possible propellant formulation into the model, and the model would provide an accurate prediction of what the burning rate chartacteristics for that mixture would be.

The physical processes involved in the combustion of solid propellants are complex, and there has been an evolutionary effort to develop models that can accurately predict their burning rate characteristics. Some of these models developed over the past 30 years are reviewed in Chapter 2, with an emphasis placed on the multiple flame-based Beckstead, Derr, and Price (BDP) model[4] and the Petite Ensemble Model (PEM)[2,6,7], the two models used as a basis for the formulation of the model which is the subject of this thesis.

Most earlier steady state composite solid propellant models have attempted to model the burning rate behavior of propellants by assuming that the propellant surface possesses "average" properties which might be observed over a long period of time. The model which is introduced herein, the Continuous Oxidizer Regression (COR) model, is an attempt to replace some of the time-averaged assumptions of earlier models, most notably the BDP model and PEM, by assuming that the propellant has a continuously regressing surface, and model the burning rate of the propellant at discrete intervals during the surface regression. Chapter 3 explains in detail the assumptions made in the COR model.

Chapter 4 contains a comparison of the theoretical predictions of the COR model with actual experimental results. Also included within this chapter is a sample of the computer-based graphical output possible with the COR model. This graphical output depicts the flame and propellant surface structures at various points in the regression of the propellant surface. Such graphical output should be helpful in developing a better understanding of the physical processes governing the burning of the propellant at different points in the surface regression. Chapter 5 contains a brief discussion of conclusions which can be drawn from this effort. Appendices A through C contain most of the finer details of the analysis which was undertaken in the development of the COR model.

CHAPTER 2 - LITERATURE REVIEW

Over the past three decades, there has been a considerable effort to theoretically model the combustion processes of composite solid propellants. The ability to accurately predict both qualitative and quantitative trends of solid fuel performance from theoretical models would be highly beneficial for rocket designers. Such models would allow a designer to tailor propellant to specific design requirements, reducing the lengthy and costly process of testing various fuels and mixtures until the right properties are found.

A composite solid propellant consists of oxidizer particles, commonly ammonium perchlorate (AP) crystals, with additional solid additives such as aluminum powder, burning rate modifiers, catalysts and acoustic suppressants, all well-mixed within a hydrocarbon fuel binder. In its simplest form, a solid propellant consists of a dispersion of oxidizer particles in a matrix of fuel binder. Even in this simplest form, the combustion of the propellant involves a multitude of subprocesses, such as fuel and oxidizer pyrolysis, melting or sublimation at the propellant surface, possible surface or subsurface interaction of the oxidizer and fuel, the formation of multiple flames, and heat transfer back to the surface. The modeler must determine which of these processes are the key processes that control propellant burning behavior, and include them within the development of any analytical combustion model.

The modeling process is also complicated by the fact that in general there will be a multitude of oxidizer particles of different sizes distributed throughout the fuel matrix Particle sizes are distributed about some mean size, and there may be several oxidizer modes, each having a different distribution of diameters about a given mean diameter. This distribution of oxidizer particle sizes is desirable because it aids in the mixing of the oxidizer and fuel during propellant formulation. However, the existence of a variety of particle sizes complicates modeling as each particle will burn with the available fuel in a different manner.

Furthermore, at any given instant on the burning propellant surface, the oxidizer particles will be at different stages of consumption. Some particles will be just beginning to burn, some will be partially consumed, and some will be almost completely consumed. An individual oxidizer particle's burning rate will vary, based upon the stage of its consumption. Therefore, a comprehensive composite solid combustion model must take this time dependent variation of burning rate of the indivual oxidizer particles into account as well.

Another complication comes about because normally, as already mentioned, there are additives in the fuel which can either enhance or suppress burning. Also, an actual propellant does not burn in a simplified test bomb but in a real rocket motor environment, wherein hot combustion gases flowing over the fuel surface can enhance its burning rate. Acoustical velocity and pressure variations set up in a rocket motor can also affect the propellant's burning characteristics. All of these effects need to be included in a comprehensive solid propellant combustion model.

Below, models representative of the evolution over the past decades especially formulated for composite solid propellants are reviewed. In the following chapter, a new approach at modeling the combustion of composite solid propellants derived from these earlier efforts will be detailed.

2.1. Granular Diffusion Flame (GDF) Model.

The first attempt at developing a theoretical model of the complex processes involved in composite propellant combustion was undertaken in the late 1950's by Summerfield and coworkers. The resulting model has been referred to as the Granular Diffusion Flame (GDF) model.[1,2] This model assumes that a thin flame zone lies very near the surface (on the order of 500 μm) as shown in Fig. 1. The burning surface is assumed to be dry, as the fuel and oxidizer gases are liberated either by sublimation or pyrolysis. The net heat release at the surface can be either exothermic or endothermic. Due to the heterogeneous

nature of the fuel/oxidizer mixture, the fuel emerges from the surface in distinct pockets of a certain mass content. These pockets then diffuse into and burn with the surrounding oxidizing medium, forming the diffusion flame zone shown in Fig. 1. The mass of these pockets is assumed to be independent of pressure, but related to the size of the oxidizer crystal. Heat transfer from the flame zone back to the surface heats up the surface resulting in the sustained gasification of the oxidizer and fuel. The diffusion process is assumed not to be turbulent, and the sole mode of heat transfer is one-dimensional conduction.
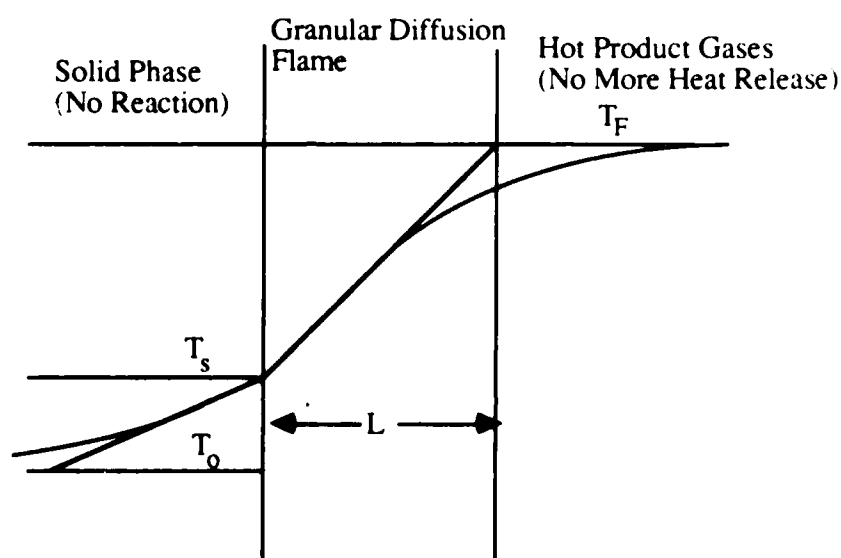
Figure 1. Summerfield's Flame Model

The burning rate or linear regression of the surface is assumed to follow an Arrhenius expression

$$r = A_s \exp\left(\frac{E_s}{RT_s}\right) \qquad (1)$$

where r is the linear burning rate, A_s is a pre-exponential frequency factor, E_s is the activation energy, R is the universal gas constant, and T_s is the surface temperature. A key component in determining the burning rate of the surface is the determination of T_s, which in turn depends on the heat transfer to the surface from the diffusion flame, Q_{Fs}, given by

$$Q_{Fs} = \lambda_g \frac{(T_F - T_s)}{L} \tag{2}$$

In Eq. (2), λ_g is the average thermal conductivity of the reactant gases, T_F is the temperature of the hot gases after the diffusion flame, and L is the distance from the surface to the thin diffusion flame. In order to obtain an accurate value for the burning rate, the heat transfer must be calculated, which in turn requires a numerical value for L, the flame height.

In determining the value of L, two extreme cases need be considered. First, at very low pressures, the rate of molecular diffusion is much faster than the rate of the chemical reaction between the oxidizer and the fuel. For this case the rate of burning in the gas phase will be controlled entirely by the speed of the chemical reaction. Second, for the case of very high pressure, the speed of the chemical reaction between the oxidizer and the fuel will be much faster than the rate of diffusion. In this case, the burning rate in the gas phase is controlled entirely by the rate of diffusion. For the low pressure kinetically limited case, Summerfield found the reaction length L to be inversely proportional to pressure causing the rate to be proportional to pressure. For the high pressure diffusion limited case, Summerfield found the reaction length L to be inversely proportional to pressure raised to the one-third power, thus causing r to be proportional to pressure raised to the same power. For the case of intermediate pressures, Summerfield assumed that the flame thickness varies partly as if it were kinetically controlled and partly as if it were diffusional controlled, resulting in the following expression for the linear burning rate r

$$\frac{1}{r} = \frac{a}{p} + \frac{b}{p^{1/3}} \tag{3}$$

In Eq. 3, a and b are constants which must be determined empirically. The parameter a accounts for the chemical kinetics effects, while the parameter b accounts for the diffusional effects, including for the first time an oxidizer particle size dependency on burning rate.

Summerfield tested this empirical correlation by first rearranging Eq. (3) to the following form

$$\frac{p}{r} = a + bp^{2/3} \tag{4}$$

If the simplistic physics within the GDF model are appropriate, then experimental plots of (p/r) versus $p^{2/3}$ should result in a straight line, with the slope of the line yielding b and the the (p/r) axis intercept yielding a. Summerfield performed experiments on the burning of a series of AP/styrene polyester resin propellants. Experimental results showed Eq. 4 to be valid over a wide pressure range for propellants of different oxidizer grinds and percent oxidizer content. Bimodal propellants were also tested, and again excellent agreement was found. Additional tests were performed using a copper chromite catalyst, and again excellent correlation was found with the form of Eq. (4).

The GDF model is still considered a valid theory for the combustion of composite propellants, and is still recommended for use in preliminary tailoring[2]. A disadvantage of the GDF model is that it is not entirely theoretical, since the parameters a and b must be determined empirically. Also, several experimentally observed effects are not well predicted or accounted for with this model, including the effect of the fuel binder type on the burning rate, the very weak effect of the oxidizer particle size on the burning rate at high pressure, the variation of the burning rate pressure exponent n (in the well-known St. Roberts expression $r = cp^n$) with ambient pressure level, especially in the region of 4000 psia, the value of the mean surface temperature of the burning propellant, and the evidence for a substantial energy release at, or very near, the propellant surface.

2.2. Hermance's Model.

Hermance[3] attempted to improve upon the GDF model, noting the shortcomings listed above. The physical-chemical surface processes incorporated in Hermance's model are the endothermic fuel binder pyrolysis, exothermic oxidizer decomposition, exothermic heterogeneous chemical reaction between the fuel binder and decomposed oxidizer in small regions surrounding the oxidizer particles, and the gas-phase combustion of oxidizer decomposition products with themselves, and combustion of the fuel with the secondary oxidizer decomposition products. Unlike the GDF model, all processes depend on either, or both, the the ambient pressure and the temperature at the point where the process in question is occurring.

Hermance assumed that the total linear burning rate at the propellant surface could be expressed as the following function of the mass fluxes from the fuel surface, the oxidizer surface, and the surface of the fuel/oxidizer reaction,

$$r = \frac{1}{\rho_T}\left[m_f(\frac{S_f}{S_T}) + m_{ox}(\frac{S_{ox}}{S_T}) + m_{sr}(\frac{S_{sr}}{S_T}) \right] \tag{5}$$

where ρ_T is the total density of the propellant and S_T is the total surface burning area. The surface areas of the fuel, oxidizer, and fuel/oxidizer interaction areas are given by S_f, S_{ox} and S_{sr} respectively, while m_f, m_{ox} and m_{sr} are the mass fluxes of the fuel, oxidizer and fuel/oxidizer surface reaction, respectively. The surface area ratios for the fuel and oxidizer were simply determined to be $(1 - \zeta_{ox})$ and ζ_{ox}, respectively, where ζ_{ox} is the volume fraction of the oxidizer. The surface area where the oxidizer/fuel surface reaction occurs is shown in Fig. 2. In this figure, the oxidizer crystal on the burning surface is shown to have decreased in dimension from its original size. This dimension change results in the

production of a fissure of depth ε between the crystal and the fuel binder. The mean planar

fuel surface shown has been assumed to intersect the oxidizer with an expected diameter of

$$D_{ox}' = \sqrt{2/3}\, D_{ox} \tag{6}$$

where D_{ox} is original diameter of the oxidizer particle.
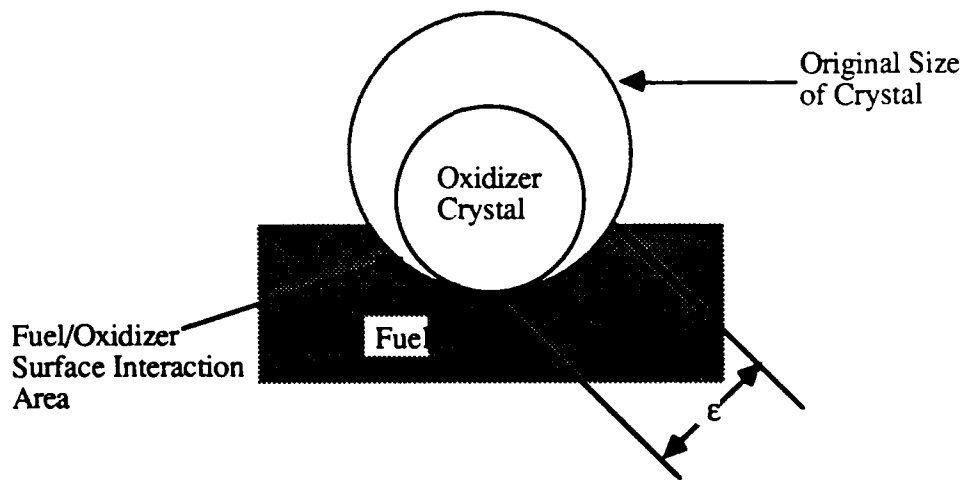
Figure 2. Fuel/Oxidizer Geometry of Hermance's Model

Assuming a bimodal propellant, the two distributions having ΔD_1 and ΔD_2 discrete

particle diameters, such that the mass fraction of oxidizer is given by α_1 and α_2, Hermance

determined that the oxidizer/fuel reaction area ratio could be given by

$$\left(\frac{S_{sr}}{S_T}\right) = \zeta_{ox}\sqrt{24}\left[\left(\frac{1-\alpha_1}{\Delta D_1 + 1}\right)\sum_{i=1}^{\Delta D_1 + 1}\left(\frac{\varepsilon_i}{D_i}\right) + \left(\frac{\alpha_2}{\Delta D_2 + 1}\right)\sum_{i=1}^{\Delta D_2 + 1}\left(\frac{\varepsilon_i}{D_i}\right)\right] \tag{7}$$

where ε_i is the fissure depth shown in Fig. 2. The ratio (ε_i/D_i) can be shown to be equal to

$$\frac{\varepsilon_i}{D_i} = V p^{\delta} \left[(\frac{C}{r}) - (\frac{K D_i^n}{p^m}) \right] \qquad (8)$$

where V, δ, C, K, m and n are experimentally determined constants.

The mass burning rate of the fuel is assumed to follow an Arrhenius burning law similar to that given in Eq. (2), while the oxidizer burning rate is related to the fuel burning rate by forcing the overall fuel/oxidizer mass ratio of the propellant to be preserved, resulting in

$$m_{ox} = (\frac{\alpha}{\zeta_{ox}}) m_T \qquad (9)$$

where α is the total oxidizer mass ratio ($\alpha_1 + \alpha_2$). Determining m_{sr} requires more complex calculations and involves consideration of the partial pressure of AP gas above the burning surface. When the expressions for m_{ox}, m_f, and m_{sr} are substituted into Eq. (5), along with the expressions for the surface area ratio, the following expression results for the determination of the surface burning rate

$$r = a_1 \exp(\frac{-E_f}{E\theta_s}) + b_1 p^{\delta} (\theta_s)^{-1/2} \left[(\frac{c_3}{r}) - (\frac{d}{p^m}) \right] \exp \left[\frac{-(E_{ox} + E_{sr})}{E\theta_s} \right] \qquad (10)$$

In Eq. (9), a_1, b_1, and c_3 are analytically determined constants, d is K times the oxidizer/fuel reaction surface area given in Eq. (7), and E_f, E_{sr} and E are the activation energies for the fuel binder pyrolysis, surface reaction, and gas phase reaction, respectively. E_{ox} is half of the activation energy for the oxidizer decomposition. The dimensionless temperature parameter θ_s is (RT_s/E).

In order to determine the burning rate, the surface temperature must be known. Energy balances are performed on Regions 1, 2, and 3 shown in Fig. 3, resulting in

equations which can be solved for the surface and flame temperatures. To solve for these two temperatures, the flame standoff distance and the net heat release at the surface of the propellant must be obtained. When equations for these two additional parameters are determined, the following equations for the dimensionless surface and flame temperatures result.

$$\theta_s = b_2 + (\frac{b_3 p^\delta}{r\theta_s^{1/2}}) \left[\frac{c_3}{r} - \frac{d_1}{p^m} \right] \exp\left[\frac{-(E_{ox} - E_{sr})}{E\theta_s} \right] - (\frac{a_2}{r}) \exp(\frac{-E_f}{E\theta_s})$$
$$+ a_3 \exp\left[\beta\theta_f^2 \log^{-1}[\frac{1}{\theta_f}](\frac{r}{p})^2 \right] \tag{11}$$

$$\theta_F = \theta_s + a_3 \left[1 - \exp\left[-\beta\theta_f^2 \log^{-1}[\frac{1}{\theta_f}](\frac{r}{p})^2 \right] \right] \tag{12}$$

a_2, a_3, b_2, b_3, and β are all analytically determined constants. Equations (10), (11), and (12) are iterated upon until consistent values for r, θ_F and θ_s are obtained.
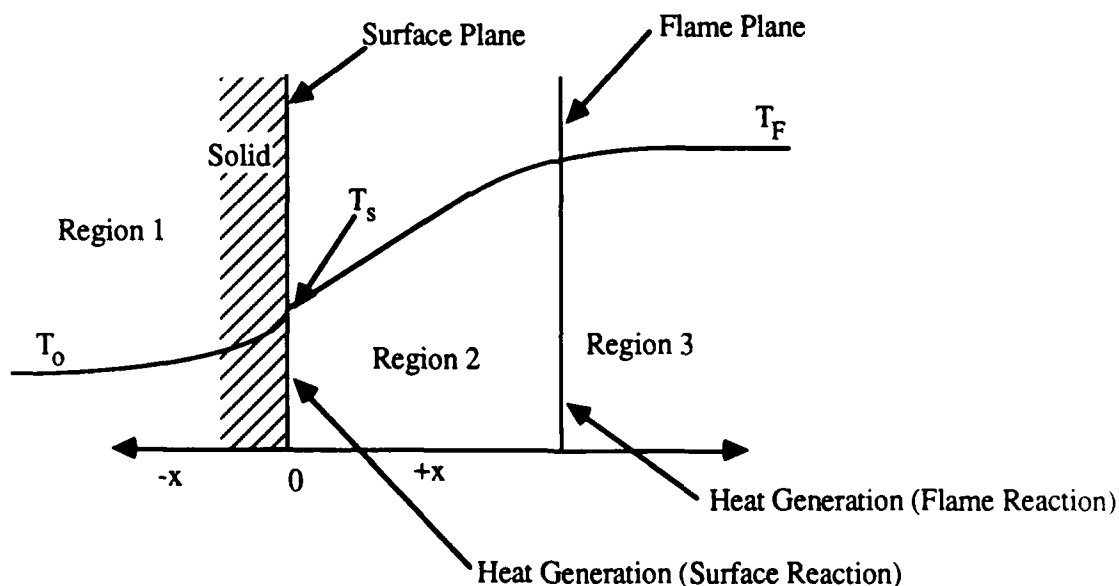
Figure 3. Sketch of Hermace's One-Dimensional Model Used to Calculate Gas and Solid Phase Temperature Distributions

Results of comparisons of Hermance's model with standard experimental results showed remarkably good agreement. A good fit with experimental data was found in the pressure range of 1 - 400 atmospheres. The theory correctly predicted the decreasing effect of oxidizer particle size on burning rate at pressures of 200 atmospheres or greater. The model correctly predicted the the experimentally observed change of the burning rate-pressure curve from concave down to concave up at pressures in excess of 100 atmospheres. Hermance's theory predicts that the burning rate exponent in the $r = cp^n$ burning law will approach a constant value at high pressure; however, experimental data shows that the pressure exponent continues to increase.

The surface geometry Hermance assumed turned out to be in error. There is no evidence that a fissure develops between the oxidizer and the fuel as shown in Fig. 2. However, Hermance's model remains a major step forward in the modeling of composite solid propellent combustion. This was the first model to incorporate the heterogeneity of the propellant surface in a purely theoretical formulation. The statistical treatment of the propellant surface, wherein a distribution of oxidizer particle sizes within the fuel matrix is assumed, as shown in Eq. (6), has been used in a somewhat different form in subsequent theoretical treatments of solid propellant combustion.

2.3. Beckstead, Derr, and Price (BDP) Model.

The next major advance in theoretical modeling of solid propellant combustion came about with the Beckstead, Derr, and Price (BDP) model.[4] This model departed from earlier models in its treatment of the flame structure formed above the propellant surface. The GDF model and Hermance's model assumed a single diffusion flame formed above the surface, while Hermance's model assumed an AP monopropellant flame occurring right at the propellant surface. The BDP model recognized that the real flame structure is more complicated than that. In the BDP model, it is recognized that the AP monopropellant flame can exist at some removed point from the surface. A diffusion flame can form below

the AP monopropellant flame as the gasified AP burns with the fuel binder, and a final diffusion flame can form above the AP monopropellant flame as fuel vapors react with secondary oxidizing products unconsumed in the AP flame. This multiple flame structure is shown in Fig. 4.
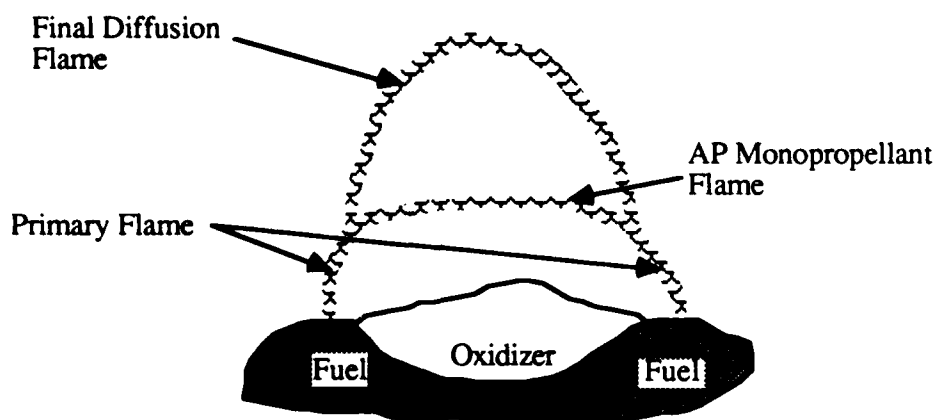
Figure 4. BDP Flame Structure

At low pressures (ambient to 100 psia) the rate controlling process is chemical kinetics, as in the GDF model, and the fuel and oxidizer have time to completely diffuse together before any chemical reaction can occur. Hence, the only flame produced is the primary diffusion flame of the fuel and oxidizer. At higher pressures, it becomes more difficult for the fuel and oxidizer to completely diffuse into one another, and the time of diffusion for fuel to the region above the center of the AP particle becomes long enough to allow the AP monopropellant kinetics to take place, and the AP flame will form over the center region of oxidizer surface. Above the AP flame, secondary oxidizing products then react with unused fuel to form the final diffusion flame. As pressure is further increased, it becomes increasingly difficult for the fuel to diffuse into the AP gas, and the AP flame will grow correspondingly larger and the primary diffusion flame correspondingly smaller. At higher pressures, where chemical kinetics can occur more rapidly, the primary AP decomposition products react almost exclusively with themselves to form the AP flame, and only a negligible fraction react with the fuel to form the primary diffusion flame.

Beckstead and his coworkers reviewed the extensive studies which had been made of the burning surface and noted that the AP crystals protrude from the burning surface at low pressures and are recessed at high pressures. The former case is shown in Fig. 4. They also noted that no evidence was found for the cusps between the oxidizer and fuel assumed in Hermance's model. These geometric findings are incorporated into the BDP model. The average oxidizer intersection diameter given by Eq. (6) is retained in the BDP model. The overall propellant burning rate is calculated based on this mean diameter.

Assuming that the regression of the oxidizer is the dominant factor in the combustion of the propellant, and assuming that the overall oxidizer/fuel mass ratio is preserved, the following expression is derived for the total burning rate of the propellant.

$$m_T = (\frac{m_{ox}}{\alpha})(\frac{S_{ox}}{S_{tot}}) \tag{12}$$

The surface area ratio in Eq. (12) is found by assuming that the oxidizer surface either protrudes above or is recessed below a planar fuel surface, and is given by

$$\frac{S_{ox}}{S_T} = \frac{\zeta_{ox}[6(\frac{h_{ox}}{D_{ox}})^2 + 1]}{6\zeta_{ox}(\frac{h_{ox}}{D_{ox}})^2 + 1} \tag{13}$$

where ζ_{ox} is the volume fraction of the oxidizer. The quantity (h_{ox}/D_{ox}) is the ratio of the average height of the center of the oxidizer surface either above or below the fuel surface to the oxidizer diameter, and is found from:

$$\frac{h_{ox}}{D_{ox}} = \frac{1}{2}(1 \pm \frac{1}{\sqrt{3}})(1 - \frac{r_{ox}}{r_f}) + r_{ox}\frac{t_{ign}}{D_{ox}} \tag{14}$$

In the above equation, t_{ign} is an empirical ignition delay time for the oxidizer particle. It is postulated that upon being exposed at the propellant surface by the regressing fuel binder, the oxidizer particle must experience this delay prior to ignition.

In order to evaluate the mass burning rate in Eq. (12), m_{ox} must be determined. The oxidizer burning rate is once again assumed to follow an Arrhenius burning law, so the surface temperature must be determined. An energy balance in the solid phase is conducted which results in the following expression for T_s.

$$T_s = T_o - \alpha \frac{Q_L}{c_p} - (1-\alpha)\frac{Q_{fuel}}{c_p} + (1-\beta_F)\alpha\left[\frac{Q_{AP}}{c_p}\exp(-\xi_{AP}) + \frac{Q_{FF}}{c_p}\exp(-\xi_{FF})\right]$$
$$+ \beta_F\frac{Q_{PF}}{c_p}\exp(-\xi_{PF}) \qquad (15)$$

In this equation, the ξ terms are dimensionless standoff distances of the AP monopropellant flame (subscript AP), the primary diffusion flame involving the fuel and gasified AP (subscript PF), and the final diffusion flame involving the fuel and secondary oxidizing products of the AP flame (subscript FF). The heat release (Q) terms are the heat of gasification of the oxidizer (Q_L), the heat of pyrolysis of the fuel binder (Q_{fuel}), and the heat released by the AP flame (Q_{AP}), the primary diffusion flame (Q_{PF}), and the final diffusion flame (Q_{FF}). The term β_F designates the fraction of the decomposing AP oxidizing reactants that are consumed in the primary flame. The relationship of this β_F parameter to the various flame standoff heights discussed below is given in Appendix C.

For a kinetically controlled flame, a standoff distance can be given by

$$x = \frac{m}{P^{\delta}A\exp(\frac{-E}{RT})} \qquad (16)$$

In this expression, m is a gas phase mass flux while δ, A and E correspond to the order, pre-exponential frequency factor, and activation energy, respectively, of the kinetic reaction

occurring at some average gas phase temperature T. For the two kinetic reactions - one for the primary flame and the other for the AP monopropellant flame - two standoff distances, x_{PF} and x_{AP}, respectively, can be determined.

Diffusional standoff distances for the primary and final flames, x_{PD} and x_{FD}, respectively, can be obtained by performing a Burke-Schumann diffusion flame analysis[5]. Such a series analysis can be used to obtain the maximum diffusion height the flame will attain above the surface. From this overall flame height, an "effective" diffusion flame height can be found by calculating the fraction of the maximum flame height at which a flat flame would be able to achieve the same heat transfer back to the surface.

The primary diffusion flame's dimensionless height ξ_{PF} is taken to be the summation of the kinetic and the effective diffusion standoff distances

$$\xi_{PF} = \frac{c_p m_T}{\lambda} (x_{PF} + x_{PD}) \qquad (17)$$

The parameter m_T refers to the total planar mass flux from the surface. The AP flame height is controlled entirely by chemical kinetics, as all species in the AP gas are assumed to be well mixed as they leave the surface. Therefore, the AP flame's dimensionless standoff height ξ_{AP} follows

$$\xi_{AP} = \frac{c_p m_{ox}}{\lambda} (x_{AP}) \qquad (18)$$

The final diffusion flame, involving secondary oxidizer products and unconsumed fuel, is at such a high temperature to begin with that there is no kinetic flame height associated with it. The final flame nondimensional standoff height ξ_{FF} is thus related to the sum of the AP monopropellant kinetic flame height and an effective final flame diffusion height

$$\xi_{FF} = \frac{c_p m_{ox}}{\lambda} (x_{AP} + x_{FD}) \qquad (19)$$

The β_F term in Eq. (15) is found by projecting the plane formed by intersection of the AP flame with the primary diffusion flame onto the surface of the oxidizer particle. Such an evaluation can be made by assuming that the diffusion flame is either parabolic or conical. The actual value for β_F will vary somewhat depending on which geometric assumption is made. Further discussion of this term is given in Appendix C wherein only parabolic diffusion flames are considered.

The heat release terms associated with the the three flames in Eq. (15) are evaluated based on adiabatic heat balances as follows:

$$Q_{AP} = c_p(T_{AP} - T_o) + Q_L \tag{20}$$

$$Q_{FF} = (\frac{c_p}{\alpha}) \left[(T_F - T_o) - \alpha(T_{AP} - T_o) + \frac{(1-\alpha)}{c_p} Q_f \right] \tag{21}$$

$$Q_{PF} = c_p(T_F - T_o) + \alpha Q_L + (1-\alpha)Q_f \tag{22}$$

In Eqs. (21) and (22), the value for T_F is assumed to be the adiabatic flame temperature. It is assumed that this temperature will be the same for both the primary and final diffusion flames.

A surface temperature-dependent Arrhenius burning rate equation for the oxidizer, along with Eqs. (12) through (22), must be solved numerically on a computer. The surface temperature (Eq. (15)) is iterated on at a given pressure p and initial temperature T_o, with a unique overall propellant burning rate r - coupled through the mass flux terms in the flame height equations - resulting. Both pressure and initial temperature can be independently varied so that the pressure and temperature sensitivities can be evaluated for a given propellant formulation.

Results from the BDP model were compared with experimental data for a series of unimodal polysulfide propellants. It was found that the model tended to overpredict the effect of oxidizer particle size on the burning rate. The authors theorized that this had to do with discrepancies in the equations for evaluating the diffusion flame heights. The effects of oxidizer mass content on the burning rate was found to be in good agreement with experimental data, as was the predicted sensitivity of the burning rate to the initial propellant temperature.

2.4. Petite Ensemble Model (PEM).

The BDP model discussed above assumed a monodisperse propellant, that is, all oxidizer particles in the propellant were of the same diameter D_{ox}. In realitiy, however, there is a distribution of oxidizer particle sizes in the propellant. This distribution of particle sizes was partially addressed in Hermance's model in determining the average size of the postulated fissure between the oxidizer and the fuel. The Petite Ensemble Model (PEM)[2,6,7], however, treats the distribution of oxidizer particle sizes in a much more thorough approach.

In describing the particle size distribution for a particular oxidizer mode, it is convenient to define two parameters which describe this distribution. These are the oxidizer mode's mean diameter, D_{ox}, and the standard deviation of the oxidizer particle sizes about this mean diameter, σ_{ox}. The mass distribution of an oxidizer grind can then be characterized by the following log normal distribution function

$$F_{ox,d} = \frac{1}{[2\pi \ln(\sigma_{ox})]^{.5}} \exp\left[\frac{1}{2}\left(\frac{\ln(D) - \ln(D_{ox})}{\ln(\sigma_{ox})}\right)^2\right] \qquad (23)$$

Integrating this distribution function from one oxidizer particle size to another yields the fraction of the total mass of the oxidizer mode which lies between these two oxidizer size limits of integration.

The average burning rate for the oxidizer mode can be calculated in one of two ways. In the first method, the burning rate is calculated by

$$r = \int_{D_{ox}} \frac{r_d F_d}{\alpha_d} d[\ln(D_{ox})] \tag{24}$$

This is a series summation of the burning rate, where the d subscript indicates quantities related to a given oxidizer size or pseudo-propellant. It has been argued that a parallel summation of the burning rate is more appropriate, so a second integration scheme proposed takes the following form

$$\frac{1}{r} = \int_{D_{ox}} \frac{F_d}{\alpha_d r_d} d[\ln(D_{ox})] \tag{25}$$

When solving Eqs. (25) or (26) on a computer, a finite number of oxidizer particle sizes is chosen, with the particle sizes distributed about D_{ox}, based on the value of σ_{ox}. For each particle size, the burning rate is calculated, and then a simple Simpson's scheme is used to perform the integration given by Eqs. (25) or (26).

For each oxidizer particle size, the scheme used for calculating the burning rate closely follows the BDP multiple flame model outlined above. The total burning rate for the given oxidizer diameter is given by the equation

$$m_T^P = m_{ox}^P \frac{S_{ox}^P}{S_T^P} + m_f^P \frac{S_f^P}{S_T^P} \tag{26}$$

where the P superscript indicates that the quantities are planar surface-based quantities, and the T superscript indicates that the quantities are total surface-based quantities. The planar surface area ratios are related to the volume fraction of the oxidizer, ζ_{ox}, which is equal to

$$\zeta_{ox} = \alpha \frac{\rho_T}{\rho_{ox}} \tag{27}$$

The two areas ratios are then described by

$$\frac{S_{ox}^P}{S_T^P} = \zeta_{ox} \tag{28}$$

and

$$\frac{S_f^P}{S_T^P} = (1-\zeta_{ox}) \tag{29}$$

The planar and total surface areas and mass fluxes for the fuel are assumed to be equal. The total oxidizer surface area is related to the planar oxidizer surface area by the average height from the surface, h_{ox}, that the oxidizer particle either protrudes above or is recessed below the fuel suface. Equation (14) gives the relation for this dimension h_{ox}. The ratio of the total oxidizer surface area to planar area is given by

$$\frac{S_{ox}^T}{S_{ox}^P} = 3[\frac{h_{ox}}{D_{ox}}]_+^2 + 3[\frac{h_{ox}}{D_{ox}}]_-^2 + 1 \tag{30}$$

where the plus subscript refers to the average height above the surface and the minus subscript refers to the average height below the surface.

The flame structure assumed in the PEM is the same as in the BDP model, and the energy balance equations are the same as well. In performing the Burke-Schumann analysis necessary to find diffusion flame heights, several assumptions are made regarding the geometry of these flames. In the Burke-Schumann analysis, it is necessary to assume that the oxidizer decomposition products issue from the surface as a circular duct centered above the oxidizer crystal. The fuel binder pyrolysis products issue in a concentric annulus

surrounding the oxidizer stream. From geometric considerations, the radius a of the oxidizer stream and the radius b of the surrounding fuel stream can be shown to be given by

$$a = \frac{1}{\sqrt{6}} D_{ox} \qquad (31)$$

$$b = \frac{1}{\sqrt{6\zeta_{ox}}} D_{ox} \qquad (32)$$

Since the Burke-Schumann analysis requires the planar mass fluxes from each tube to be equal, the PEM allows for the inner tube radius to vary instantaneously as the gas leaves the surface via a flow slipline so that the oxidizer and the fuel mass fluxes are equal. The new inner radius a' is given by

$$a' = a \left(\frac{\alpha}{\zeta_{ox}}\right)^{1/2} \qquad (33)$$

The diffusion flame height is then solved for based on this geometry.

As in the BDP model, the surface temperature is iterated upon until convergence is obtained. Then, the burning rate for the next diameter, or pseudo-propellant, is determined. When the burning rates of all diameters have been calculated, Eq. (25) or Eq. (26) is solved to find the total propellant burning rate of the oxidizer mode.

The PEM has been modified to handle the effects of aluminum additives in composite solid propellants. This modification to the PEM is know as the ALPEM. The ALPEM models the burning process of an aluminum particle, including the heating up of the particle as it enters the thermal profile of the propellant below the surface, its further heatup and melting as it reaches the surface, its lifting off the surface by viscous drag forces of the emitting fuel gas stream, and its final ignition above the oxidizer surface. The added energy that aluminum particle combustion adds to the gas phase is taken into account in the

ALPEM in the heat transfer analysis used to determine the surface temperature. The ALPEM accounts for the existence of a distribution of sizes in the aluminum particles by solving for the heat transfer associated with each particle size, averaging the results, and using this average heat transfer value in in the energy balance used for each oxidizer particle size.

In a real rocket motor, the burning rate can be enhance by the phenomenon of erosive burning, as hot exhaust gases flowing over the surface enhance the mixing in the gas phase. The PEM can model this erosive burning enhancement, for turbulent flow across the surface. In addition, the PEM is set up to model the response of the propellant to both pressure and velocity oscillations which can be present within the rocket motor.

The PEM predictions are excellent (within ±10% of experimentally obtained burning rates and pressure exponents for a series of multi-modal non-aluminized propellant formulations). It represents a new philosphy in the theoretical modeling of composite solid propellants in its statistical treatment of real rocket fuels. While the statistical treatment of the propellant employed by the PEM will not be incorporated in this thesis, the heat transfer and flame analysis used by the PEM will be used in development of a modified burning model, which will be described shortly.

2.5. King Formulations.

Instead of assuming all oxidizer particles are of some average size, the PEM addresses the nonuniformity of oxidizer particle sizes in its statistical approach to finding an average burning rate. However, in determining the burning rate associated with each individual particle diameter, averaged parameters are used. The surface diameter of the oxidizer particle is assumed to be an average value (see Eq. (6) above), as is the height of the oxidizer above or below the fuel surface. In reality, of course, the exposed surface area is constantly changing, as well as the height above or below the fuel surface.

The tradeoffs of adopting different approaches to the modeling of solid propellant combustion was discussed by Glick[7]. Glick recognized that a model which accounts for each microstate of the oxidizer particle, i.e., each state the particle goes through as it and the fuel surrounding it are consumed, would be the most realistic modeling approach to take. However, Glick stated that in the tradeoff between model accuracy and cost and computing time, the PEM approach, which applies a statistical approach to computing the overall burning rate, but averages geometric parameters for each individual particle, was the best approach to take.

Taking the more detailed approach, King[8] developed a model to determine the burning rate of solid propellants (with oxidizer particles all of the same diameter) by averaging burning rates as the burning surface passes through a number of discrete heights (approximately 20) from the top of the oxidizer particle. The propellant is allowed to burn down to the first height increment, where the burning rate is determined, and then is allowed to burn down to the next height, where the burning rate is again determined, and so on. When the oxidizer or fuel has been completely used up, an averaging technique is used to find the the overall burning rate.

At each height from the surface, the local fuel/oxidizer geometry must be determined. Straightforward geometric evaluation can give the planar surface area of the oxidizer at any height from the top of the particle, assuming the particle is a sphere. To determine the fuel diameter, King assumed the oxidizer crystals are arranged in a closest cubic packing array, though with the spacing between particles larger than that required for 100 percent of maximum theoretical loading. Based upon this oxidizer packing arrangement, the fu⸱' surface area is apportioned to the oxidizer particle at each incremental height from the surface. When two layers of oxidizer overlap, fuel is apportioned between them based upon the ratio of the two oxidizer planar surface areas. King does not explain in detail how these assumptions are used to derive formulas to find the fuel surface area, or what these formulas are.

The fuel is asssumed to regress in a planar mannar, while the oxidizer surface is forced to be continuous at the oxidizer/fuel interface. Since the oxidizer is allowed to burn at a different rate from the fuel, the oxidizer surface can assume a curved shape, which either rises above or is recessed below the fuel surface, depending upon its burning rate relative to the fuel's burning rate. The nonplanar surface area of the oxidizer is calculated from

$$S_{ox} = \pi[\delta_{ox}D_{ox} - 2\delta_{ox}h_f + \delta_{ox}^2] \tag{35}$$

where S_{ox} is the nonplanar oxidizer surface area, h_f is the distance to the planar fuel surface from the initial top of the oxidizer particle, and δ_{ox} is the height of the center of the oxidizer surface from initial top of the oxidizer particle. This nonplanar oxidizer surface area is important as it is used in the calculation of mass fluxes and flame heights in the model.

Unlike the BDP and PEM models, King's model assumes two flames form above the burning surface, an AP monopropellant flame and a diffusion flame. King's flame model is shown in Fig. 5. Allowances are made in the AP flame computations to account for the fact that some of the AP reactants have already been consumed in the columnar diffusion flame which occurs below the point of AP flame ignition. King uses a modified Burke-Schumann analysis to determine the height of the diffusion flame above the surface. The height of the flame above the surface is modified to account for the effects of erosive burning, by assuming that the hot gases flowing parallel to the propellant surface cause the diffusion flame to be bent at some angle, reducing the perpendicular height of the flame from the surface. This bending of the flame will reduce the effective flame height, thus enhancing the burning rate of the fuel. Also, rather than computing some average standoff distance for the diffusion flame from which heat release is assumed to take place, King assumes a continuous heat transfer from the diffusion flame back to the oxidizer surface. In addition, it is assumed that the fuel and oxidizer receive different amounts of heat from

the two flames, where the fuel only receives heat from the diffusion flame while the oxidizer receives heat from both the diffusion and AP monopropellant flames.
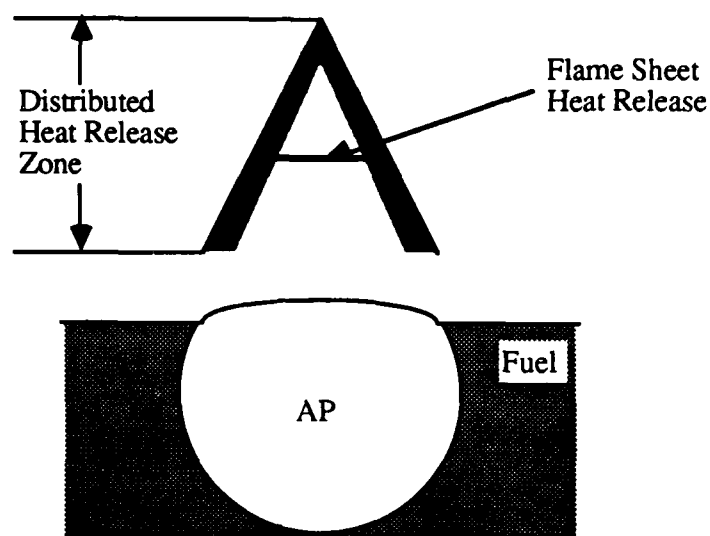
Figure 5. King's Flame Model

Also unlike the BDP or PEM, King assumes a subsurface reaction between the oxidizer and fuel which is temperature dependent. The amount of fuel and oxidizer available for flame formation in the gas phase is modified to account for this subsurface reaction.

King's entire analysis comprises 27 unknowns in 27 equations which are all solved simultaneously. In this manner, the burning rate is calculated for each height increment from the surface. To determine the average burning rate for the entire oxidizer particle, King uses the following equation

$$r_{ave} = \frac{\sum_{i}(m_{ox,i}S_{ox,i} + m_{f,i}S_{f,i})}{\rho_T \sum_{i}(S_{ox,i} + S_{f,i})} \qquad (36)$$

where S_{ox} and S_f are planar oxidizer and fuel areas and the oxidizer mass flux term m_{ox} is the based on the planar surface area of the oxidizer. The term ρ_T refers to the total density of the overall propellant. The summation above is over each of the ith individual burning states the oxidizer passes through. Other possible averaging techniques were considered, one of which will be detailed below in the discussion of the various modifications King has made to his basic model.

Use of Eq. (36) to calculate the burning rate begs the question of what happens when the oxidizer burns out before the fuel does. (King claims that geometric arguments show that the reverse situation cannot occur, but goes into no detail showing this.) King refers to this question as the "end game." When there is unused fuel left over, Eq. (36) has a number of increments for which the burning rate is zero, which will pull the average burning rate down. King keeps these terms of zero burning rate in Eq. (36), though recognizing that the issue of how to handle the question of the "end game" is far from closed.

King compared results from this model with experimental results for zero crossflow and crossflow cases. Two parameters in King's model, relating gas flame reaction distances to gas phase velocity away from the surface and pressure, were varied to search for optimal values. For the zero crossflow cases, good agreement was found with experimental results for 5 and 20 micron diameter AP propellants, but burning rates for a 200 micron AP propellant were severely underpredicted. King theorized the problem was with the rate constant used for the subsurface oxidizer/fuel reaction or that a more realistic model was needed for the heat transfer back from the diffusion flame. When the subsurface burning rate constant was varied to fit an optimal value, better agreement for the 200 micron case was found. In all cases, the predicted sensitivity of the burning rate to crossflow velocity was somewhat less than observed experimentally.

King produced another paper[9] which included a number of modifications to his original two-flame oxidizer/fuel regression model. The zero crossflow modifications

included a new method to calculate flame heights, replacing the oxidizer/fuel subsurface heat release term by a heat release term which occurs only in a surface melt layer, and a revised diffusion flame heat release term.

Two versions of this zero crossflow model were compared with experimental results. In the first version, the flame temperature and gas phase heat capacity were assigned values based on the overall oxidizer mass fraction of the propellant, instead of being based on the gas phase oxidizer mass fraction at each incremental step. Also, the average burning rate given by Eq. (36) was modified to include only those height increments with nonzero burning rates. In the other version, the oxidizer/fuel mass ratio of the gas streams emanating from the surface at each incremental height from the surface was forced to be the same as the overall propellant's oxidizer/fuel mass ratio. This made the fuel area at each incremental height from the surface equal to

$$S_f = \frac{(1-\alpha)m_{ox}S_{ox}}{\alpha m_f} \tag{37}$$

where S_f is the fuel surface area and α is the weight fraction of the oxidizer. This approach eliminates the problem of the "end game" since the fuel area is now zero only when the oxidizer area is zero. Also, using this second approach, the average burning rate is now calculated from the expression

$$r_{ave} = \frac{D_{ox}}{\sum_i \tau_i} = \frac{D_{ox}}{\sum_i \frac{\Delta\delta_{ox,i}}{r_{ox,i}}} \tag{38}$$

where τ_i is the time it takes for the oxidizer to burn through each ith incremental height and $r_{ox,i}$ is the oxidizer regression rate at each incremental height from the surface. Both of these versions showed excellent correlation with experimental data, although the first version's agreement with experimental data was found to be better.

King also developed a version of his model to handle propellant formulations where more than a single oxidizer diameter is present. To do this, King replaced the surface regression analysis with average surface area values, much the same as is done in the PEM. He then calculated the burning rate one time for each oxidizer diameter present in the fuel based on these average values, and used a "petite ensemble" approach to determine the overall propellant burning rate, again much as is done in the PEM. This model retained the "bent flame" assumption for erosive burning analysis, but also included an analysis of erosive burning enhancement of transport phenomena, once again similar to what is done in the PEM. This erosive burning model was found in general to be in good agreement with experimental data.

In the next chapter, a detailed description of how the Petite Ensemble Model (PEM) has been modified to better represent the actual time dependent burning rate behavior of a single oxidizer/fuel pair will be presented. This model, subsequently referred to as the Continuous Oxidizer/Regression (COR) model, blends the methods discussed by King into the statistical treatments and burning rate analyses employed by the PEM and earlier models discussed herein.

CHAPTER 3 - MODEL DESCRIPTION

The theoretical combustion model which is the subject of this thesis, the Continuous Oxidizer Regression (COR) Model, employs major components of the earlier Petite Ensemble Model (PEM)[2,6,7] in determining the surface temperature and burning rate of a composite solid propellant. As with the earlier PEM formulation, a surface temperature is first assigned, from which, assuming Arrhenius expressions for reaction rates, mass fluxes from the oxidizer and fuel binder surface are determined. Three types of flames may form above the surface, an AP monopropellant flame, a primary diffusion flame, and a final diffusion flame. Surface mass fluxes and the oxidizer/fuel surface geometry determine which flames form and what their heights above the surface and gas phase temperatures are. The heat fluxes from these flames back to the propellant surface are calculated, and an energy balance is performed at the surface. Based upon this energy balance, a value for the surface temperature is calculated. The calculated value is compared to the assumed value, and if the two values differ by more than an acceptable tolerance, the value for the surface temperature is adjusted, and the analysis repeated. This process is continued until convergence on a surface temperature and a corresponding burning rate is achieved. The COR model has incorporated new assumptions into the basic framework of the PEM in an attempt to more realistically model the combustion of a solid propellant. These new assumptions are to be discussed in this chapter.

3.1. Oxidizer/Fuel Geometries.

In the original PEM, it is assumed that for the mean combustion state of a typical oxidizer/fuel binder pair, the oxidizer surface exists some average height either protruding above or recessed below the planar fuel surface. This height is based upon an assumed ignition delay period, which was discussed in Chap. 2. Based upon this ignition delay time and the concept of a mean combustion state representing the entire oxidizer particle

burning process, an average surface diameter of the oxidizer particle and the average height of the oxidizer surface above or below the fuel surface are calculated. These values are then used to determine the average nonplanar surface area of the oxidizer particle. The ratio of the planar to nonplanar oxidizer surface areas gives the correction factor by which the nonplanar oxidizer mass flux (given by Arrhenius kinetics) is multiplied in order to represent an actual surface planar oxidizer mass flux. Based upon the propellant oxidizer-to-fuel mass ratio, a fuel surface diameter corresponding to the average oxidizer surface diameter is calculated. These two average diameters then become the diameters of the inner and outer tubes of issuing fuel and oxidizer needed to calculate the height of the primary and final diffusion flames above the propellant surface. With known surface geometry along with the fuel and oxidizer surface mass fluxes, gas temperatures, and other thermophysical constants, kinetic flame heights above the propellant surface are also obtained.

One of the major departures from the PEM formulation that distinquishes the COR model is that the burning surface of a single oxidizer/fuel binder pair is assumed to continually regress. No longer is the overall oxidizer particle burning rate assumed to be represented by the burning rate of a single mean state oxidizer/fuel geometry. The burning rate is therefore calculated at a number of discrete intervals; the burning rate for each interval being determined by the local fuel/oxidizer geometry over that interval. Therefore, the mean state/average surface geometry assumptions of the PEM are disregarded, and instead, a surface geometry and instantaneous burning rate is determined at discrete time intervals during the overall oxidizer/fuel binder pair combustion.

The first assumption which needs to be made in the COR model is the geometric relationship between the oxidizer particle and the planar fuel surface which effectively engulfs it. The oxidizer particle is assumed to be spherical in all cases considered. Two possible senarios for allocating the fuel surrounding an individual oxidizer particle are assumed. In the first scenario, the available fuel surrounds the oxidizer as a concentric

sphere, as shown in Fig. A.1. Such a configuration assumes that the fuel binder equally "wets" the individual oxidizer particles. The other possible scenario is one in which, at any planar cut through the oxidizer particle, the fuel and oxidizer are always in the same mass ratio as that of the overall propellant. This restriction results in the configuration shown in Fig. A.5. This is stating that an oxidizer/fuel binder pair always burns at a constant stoichiometry throughout with only the relative geometric dimensions changing.

The discreet time intervals at which the COR model calculates a burning rate are the incremental times during which equal volumes of fuel have been consumed. As in the PEM, the fuel surface is always assumed to remain planar, so as each volume of the fuel is consumed, a different planar surface will become exposed. The planar fuel and oxidizer diameters at these intervals will depend on what the height is from the initial planar surface when a given volume of fuel has been consumed. The details of how the height from the initial planar surface and the new planar fuel and oxidizer diameters are determined are presented in Appendix A below.

In the COR model, the oxidizer and fuel are allowed to burn at different rates; the burning rates being determined by different Arrhenius burning rate constants. The oxidizer surface must remain continuous with the fuel at the point where the oxidizer and planar fuel surfaces intersect, and this restriction causes the oxidizer surface to assume the shape of a partial sphere which either protrudes above or is recessed below the planar fuel surface. Whether the oxidizer surface lies above or below the planar fuel surface depends on whether the oxidizer is burning slower or faster than the fuel. For the results presented herein, the COR model assumes a single surface temperature represents both the oxidizer and fuel binder. However, like the PEM, a separate surface temperature approach can be utilized.

An oxidizer burning mass flux is determined from an Arrhenius expression, and when divided by the oxidizer density, the linear oxidizer burning rate results. This burning rate is then multiplied by the time the incremental fuel volume takes to be consumed, and

this product is gives the vertical distance that the center of the oxidizer surface has regressed. This displacement is subtracted from whatever the previous oxidizer height from the original surface was, and a new height of the oxidizer surface from the original surface is determined. The difference between this height and the instantaneous fuel surface displacement determines whether the oxidizer surface lies above or below the fuel surface. Once the height of the oxidzer surface above or below the fuel surface is determined, the oxidizer's nonplanar surface area is determined. As is the case with the PEM, this ratio of the planar area to the nonplanar surface area provides a correction factor which the oxidizer's burning mass flux is multiplied in order to determine the total planar oxidizer mass flux from the surface.

Even though the surface geometry is calculated only at discrete intervals, the fuel is in fact being consumed continuously. Therefore, over any given burning increment, it is necessary to take averages of what the oxidizer diameter, fuel diameter, and nonplanar oxidizer surface area are during that time increment. Appendix A provides all the necessary details on how these average quantities are determined.

3.2. Flame Structures.

In the PEM model, it is reasonable to assume that the diffusion flames that form are almost always under-ventilated for the typical values of the propellant oxidizer mass fraction, α, considered and, therefore, close over the oxidizer surface. However, in the COR model, where the surfaces are continuously regressing, a highly nonplanar, time dependent oxidizer surface can result. The corrected mass flux from this nonplanar burning surface can be large enough so that both the primary and final diffusion flames become over-ventilated (closing over the fuel binder surface).

Even though the PEM assumes that the oxidizer surface is nonplanar when the oxidizer mass flux is being calculated, for geometric simplicity the formation of flames is still considered to occur over a flat surface. In the COR model, the effect that the nonplanar

oxidizer surface has on the formation of flames is taken into account. This effect, plus the effect of whether the diffusion flames are over- or under-ventilated, leads to the possible flames cases shown in Figs. 6 through 10.

The first possible flame case, Case A, is shown in Fig. 6. This case occurs when the oxidizer surface is concave (recessed below the planar fuel surface), and the standoff distance for the AP monopropellant flame, x_{AP}, is smaller than the maximum depth of the oxidizer surface below the fuel surface, h_{ox}. (Appendix A shows in detail how the quantity h_{ox} is calculated). The AP flame is assumed to be a flat flame sitting at a distance of $(h_{ox} - x_{AP})$ below the planar fuel surface, and extends horizontally to the points where it touches the oxidizer surface. It is assumed that the fuel cannot diffuse below the planar surface to react with the oxidizer, so no primary diffusion flame forms. A final diffusion flame begins just at the planar surface, where the fuel first has the chance to react with the AP flame products. The final diffusion flame may either be over- or under-ventilated depending on the overall oxidizer/fuel stoichiometry.

The question arises as to whether the AP flame should in fact be assumed to be flat, since oxidizer is issuing from a continuous nonplanar surface. Although the assumption that the flame is indeed flat and sits at a height of x_{AP} above the bottom of the oxidizer surface is clearly not precise, it does account for the fact the oxidizer-rich AP monopropellant flame combustion products that take part in the final diffusion flame are issuing from below the fuel surface. Determining what the actual shape and location of this flame is beyond the scope of this effort, so the flat flame approximation is used here out.

The second possibility for flame formation is shown in Fig. 7. This case (Case B) is again for a concave oxidizer surface. Now the AP flame is of such a height that when compared with h_{ox}, the AP flame is observed to sit above the planar fuel surface. The primary diffusion flame would now have a chance to form except that in this case, the primary flame's kinetic standoff height, x_{PF}, is greater than the vertical location of the AP flame, $(x_{AP} - h_{ox})$. The primary flame has no chance to develop, since all of the oxidizer

decomposition products are used up in the AP monopropellant flame before a primary diffusion flame reaction can ever occur. As always, a final diffusion flame forms above the AP flame, and can either be over-ventilated or under-ventilated.

If the value of $(x_{AP} - h_{ox})$ grows larger than the primary flame's kinetic standoff height, x_{PF}, then a primary diffusion flame can begin to form. This case (Case C) is shown in Fig. 8. The primary diffusion flame will be cut off at the point $(x_{AP} - h_{ox})$, since no oxidizer will be available to the primary flame beyond this point. For the under-ventilated case, the AP flame will extend horizontally to the points where it cuts off the the primary diffusion flame. The final diffusion flame then forms above the AP flame.

For the over-ventilated case, the primary flame will still be cut off at the height above the surface where the AP flame forms. Since part of the oxidizer decomposition products are used up in the primary flame, the AP flame only extends a horizontal distance $(1 - \beta_F)D_{ox}$, where β_F the fraction of reactants entering the primary flame, is determined as shown in Appendix C. Physically, is it clear that a diluted AP flame should extend all the way to the points where it cuts off the primary flame, but from a heat transfer standpoint, this assumption is equivalent to considering the AP flame to have an extent of $(1 - \beta_F)D_{ox}$, since only $(1 - \beta_F)$ of the original oxidizer will ever be able to react in the AP monopropellant flame. Since the end goal of the flame formation analysis is to determine the heat transfer back to the propellant surface, the assumption of the AP flame having of diameter of is $(1 - \beta_F)D_{ox}$ is valid.

A limiting value in the formation of an AP flame is reached when $(x_{AP} - h_{ox})$ equals $(x_{PF} + x_{PD})$, where x_{PD} is the fully developed primary diffusion flame height. Beyond this point, the primary diffusion flame has the opportunity to completely develop and close over the fuel or oxidizer surface, and this will be the only flame which forms, since there is no oxidizer available to form an AP monopropellant flame.

The cases where the oxidizer surface is convex (protruding above the planar fuel surface) now need to be considered. For these cases, the AP monopropellant flame is

assumed to always lie at the height x_{AP} above the oxidizer suface, leading to a curved AP flame matching the contour of the oxidizer surface. This assumption can be questioned just as the assumption of a flat AP flame when the surface is concave can be questioned. The oxidizer is in fact discharging mass normal to the AP surface whose slope is constantly changing, so in all likelihood such gases will not travel in a perfectly vertical direction before combustion. The assumption does, however, account for the nonplanar nature of the AP surface, and with no information available as to what the actual flame contour would look like, assuming that the flame matches the oxidizer surface appears to be a reasonable assumption.

The first case to be considered when the oxidizer surface is convex, Case D, is shown in Fig. 9. For this case, $(x_{PF} + x_{PD})$ is less than h_{ox} and it is assumed that the oxidizer surface acts as a "wall" which will keep the fuel from diffusing inward to react with the oxidizer. Therefore, if the diffusion flames are under-ventilated, the primary flame never gets a chance to form, and only the AP and final diffusion flames form. However, if the flames are over-ventilated, the primary diffusion flame can form. For the over-ventilated case, following the same line of reasoning as in the case of a concave oxidizer surface, the AP flame will not extend to the point where the primary diffusion flame is cut off, but will only extend the horizontal distance $(1 - \beta_F)D_{ox}$.

In Case E, shown in Fig. 10, x_{PD} is now greater than h_{ox}, and x_{PF} is less than x_{AP}. The oxidizer surface now no longer acts as a barrier to the formation of the primary diffusion flame, and since x_{PF} is smaller than x_{AP}, the primary diffusion flame has a chance to form. There are two extreme limits to Case E. If x_{PF} grows larger than x_{AP}, no primary diffusion flame will form, and the only flames formed will be the AP monopropellant and the final diffusion flames. If x_{AP} grows larger than $(x_{PF} + x_{PD})$, no AP flame will form, and the only flame formed will be the primary diffusion flame.

It is noted that while the assumption of a nonplanar oxidizer surface is used in determining which flames will form, the effective heights of the flames used in the heat

transfer analysis to obtain a surface temperature (Eq. 15), are always the flame heights relative to the planar fuel surface. The three-dimensional analysis that would be required to determine what the effective height of a flame is relative to the nonplanar oxidizer surface, and what fraction of the heat of this flame goes to this surface and what fraction goes to the fuel surface, is beyond the scope of the present analysis.

3.3. Incremental Surface Temperature Calculation.

The burning rates calculated for the fuel and oxidizer at each discrtete interval are based upon an assumed surface temperature. To determine whether this surface temperature is correct, a surface energy balance must be performed. If the assumed surface temperature does not agree with the temperature resulting from the surface energy balance, then it must be modified until it is sufficiently close to the value returned by the surface energy balance.

The COR model's energy balance equation is the same as that used in the BDP and PEM models, Eq. (15). It assumes the same type of multiple flame formation above the propellant surface as the PEM does. The criteria used to determine which types of flames will form for a given oxidizer/fuel geometry are modified in the COR to account for nonplanar effects, as explained in Sec. 3.2 above.

The heat transfer analysis of Eq. (15) assumes a single surface temperature for both the oxidizer and fuel surfaces. The energy balance is performed with respect to the oxidizer surface, and it is assumed that the fuel surface will have the same temperature. As already mentioned in the discussion of flame formation, the three-dimensional analysis required to determine the heat flux back to the fuel and oxidizer surface, and the subsequent dual energy balances required for both of these surfaces, will not be included within the scope of the current investigation.

The heat transfer analysis requires a knowledge of which flames form above the planar surface, along with information as to the heights of these flames above the oxidizer

surface. Section 3.2 outlines the logic used to determine which flames are formed. The representative flames heights are determine as described below.

When the AP monopropellant flame exists, its height above the surface is taken as the kinetic standoff height of the flame. This assumption is employed when the oxidizer surface is concave (recessed) because even though the flame height lies at $(x_{AP} - h_{ox})$ above the planar suface, it still will be located at x_{AP} above the center of the oxidizer surface, and the heat transfer analysis is performed with respect to this surface. When the oxidizer surface is convex (protruding), the AP flame lies at x_{AP} above the surface at every point along the surface, so no correction for the height is warranted.

The calculated diffusion flames are assumed to be parabolic in shape, so determining the heat transfer from this type of flame back to the oxidizer surface is more complicated. The PEM calculates an equivalent standoff distance at which a flat flame would have to exist to produce the same heat transfer as the parabolic diffusion flame produces. This equivalent standoff distance is then added to the kinetic height of the flame for the primary diffusion flame or added to the kinetic AP monopropellant flame height for the final diffusion flame. These overall flame heights are then used in their nondimensional form within the surface energy balance, Eq. (15).

As mentioned previously, the PEM calculation of the equivalent flat flame standoff distance is used assuming that the diffusion flame is almost always under-ventilated (closing over the oxidizer surface). In the COR model, however, over-ventilated diffusion flames (closing over the fuel binder surface) are also a possibility. The heat transfer analysis required to find the equivalent standoff distance for an over-ventilated flame is different from that performed on an under-ventilated flame. This analysis is given in Appendix B below.

The β_F parameter in Eq. (15) is the fraction of reactants which react in the primary diffusion flame when such a flames develops. The equation for β_F for the case of an under-ventilated flame is given by Eq. (C.1). It is based upon the kinetic heights of the

primary and AP monopropellant flames, and on the height of the primary diffusion flame. This equation needs to be modified for the case of an over-ventilated flame. This analysis is shown in more detail in Appendix C.

The PEM calculates the adiabatic flame temperatures required in Eq. (15) based on the overall oxidizer/fuel mass ratio of a given pseudo-propellant or oxidizer/fuel binder pair. In the COR model, the adiabatic flame temperatures are determined based upon how much fuel and oxygen are consumed during a given burning increment. The mass of fuel consumed for a given burning increment will be constant, since each burning increment is defined as the time it takes for a fixed volume of fuel to be consumed. To find the mass of oxidizer consumed, it is necessary to know the time it takes for this volume of fuel to be consumed.

The time it takes for the fuel volume to be consumed is the product of the fuel's burning rate times the horizontal distance its planar surface must regress in order for the given fuel volume to be consumed. Due to the spherical geometry involved, this horizontal distance will not be the same for each subsequent equal volume of fuel consumed, but will depend on the location of the fuel being consumed relative to the initial planar surface. The calculation of these incremental horizontal distances is covered in Appendix A. Once the horizontal distance which the fuel surface has regressed is determined, the time it takes for the fuel to be consumed is simply this horizontal regression distance divided by the fuel's average burning rate. The fuel's average burning rate is determined by averaging the burning rate for the current marching increment (based on an Arrhenius expression and the assumed surface temperature) with the burning rate that was calculated at the previous marching increment.

The incremental distance that the oxidizer regresses is found by multiplying the time it takes the fuel to be consumed by the burning rate of the oxidizer (again calculated based on an Arrhenius expression and the assumed surface temperature) averaged with the burning rate from the previous marching increment. This incremental distance is then subtracted

from the horizontal location of the oxidizer at the previous burning interval to obtain the new horizontal location of the oxidizer surface. Based upon this new horizontal location of the oxidizer surface, and its relative location with respect to the planar fuel surface, the parameter h_{ox} can be found. From the value of h_{ox}, the volume of oxidizer consumed, and its respective mass, can be calculated. The additional details of the calculation of the volume of oxidizer consumed are given in Appendix A. The mass of fuel consumed follows directly from the volume of fuel consumed, and the adiabatic flame temperature can then be found from the oxidizer/mass ratio.

Once it is determined which flames form above the surface, what the flame heights and flame temperatures are, and what percentage of the reactants are consumed in each flame, Eq. (15) can be used to calculate a new surface temperature. If the new surface temperature is not sufficiently close to the assumed value, a new surface temperature is selected and the flame formation/heat transfer analysis is performed again. This process is continued until convergence is achieved on the proper surface temperature. The time it takes the volume of fuel to be consumed based on this surface temperature is added to the burning times from previous burning increments, to obtain a new total burning time. The burning rates of the fuel and oxidizer for the current burning interval are stored and used in determining the average burning rates at the next burning interval.

3.4. Oxidizer Crystal Marching Scheme.

It is assumed that at the initial point of the burning analysis, when the tip of oxidizer particle has just been exposed at the planar fuel binder surface, the burning rate is effectively zero. At each succeeding increment below this initial surface, the incremental burning rates for the fuel and oxidizer and the incremental burning time are determined as described in Sec. 3.3 above.

This procedure continues up to the point where either the fuel binder or oxidizer is completely consumed. It is possible that one of these propellant constituents can burn out

before the other due to the fact that they have different burning rates. If the allocated fuel binder burns out before the oxidizer does, the final burning area for the fuel will be zero. The burning rate for the fuel at the end of the final increment must therefore be zero. To compute the burning time for this final increment the burning rate of the fuel from the previous time step is divided by two to obtain an effective average burning rate. This average burning rate is used to calculate the burning time of the final increment. As before, this burning time is added to the burning times of the other increments to obtain the overall burning time.

If the oxidizer burns out before the fuel does, then for the increment in which the oxidizer burns out, the oxidizer will be completely consumed before or just when the incremental volume of fuel has been consumed. Once the oxidizer is completely consumed, it is again assumed that the burning rate for the fuel is zero. Therefore, the height increment for this interval must be based on how much fuel was consumed just prior to the oxidizer completely burning out. For this final burning interval, a burning time must be calculated based upon how long it takes for the oxidizer to burn out. This burning time will be the inverse of burning rate of the oxidizer divided by the distance the oxidizer regresses before it burns out. Based upon this burning time, and the linear burning rate of the fuel, the distance the planar fuel surface regresses can be calculated. The volume of fuel consumed can be found from this distance by the methods shown in Appendix A. The volume of oxidizer consumed will be the volume of oxidizer that remained at the beginning of the burning increment. All values needed for a surface energy balance over the final burning increment are then known. When convergence on a surface temperature is achieved, the burning time for the fuel is added to the previous total burning time to obtain the updated total burning time.

3.5. Overall Burning Rate Calculation.

At the beginning of the COR analysis, when the oxidizer particle has first been exposed to the surface, the total burning time is taken to be zero. After the burning rate analysis has been completed for the first incremental volume of fuel consumed, the time it takes for the fuel to be consumed over this increment becomes the total burning time of the propellant. After the burning rate analysis has been completed for the second volume of fuel consumed, the time it takes for the second volume to be consumed is added to the total burning time, and this sum becomes the new total burning time. This process is continued until the analysis on the last burning increment has been completed.

The COR model requires that the fuel and oxidizer burn in the same proportion as the oxidizer/fuel mass ratio of the overall propellant. If, after the oxidizer or fuel has burned out, the ratio of the total mass of fuel burned to the the total mass of oxidizer burned is not in agreement with the overall oxidizer/fuel mass ratio, then the value of oxidizer mass fraction α used in Eq. (A.1) is adjusted so that a greater or lesser mass of fuel surrounds the oxidizer crystal. If the ratio of oxidizer to fuel burned is less than the required ratio, then the total volume of fuel surrounding the oxidizer is decreased, so that when the oxidizer or fuel burns out, less fuel will have been consumed. If the ratio of oxidizer to fuel burned is greater than the required mass ratio, then more fuel should be apportioned to the oxidizer, so that when the oxidizer or fuel burns out, more fuel will have been consumed. This process is continued until convergence is achieved.

After the proper apportioning of fuel to the oxidizer described above is achieved, the overall oxidizer/fuel binder pair burning rate is calculated from the following expression.

$$r = \frac{D_{ox}}{t_T} \tag{39}$$

In Eq. (39), r is the total burning rate, t_T is the sum total burning time over all the burning increments, and D_{ox} is the diameter of the oxidizer particle for the oxidizer/fuel binder pair under consideration.

This equation for the burning rate begs the question of what happens to the fuel or oxidizer left over. It is assumed that the left over fuel, if there is any, is used in the burning process of the other oxidizer particles within the propellant formulation. If there is any oxidizer left over, it is assumed that the remaining crystal simply lifts off the surface once its surrounding fuel is consumed and does not contribute anything more to the burning of the propellant. In both instances, overall propellant stoichiometry is perserved.
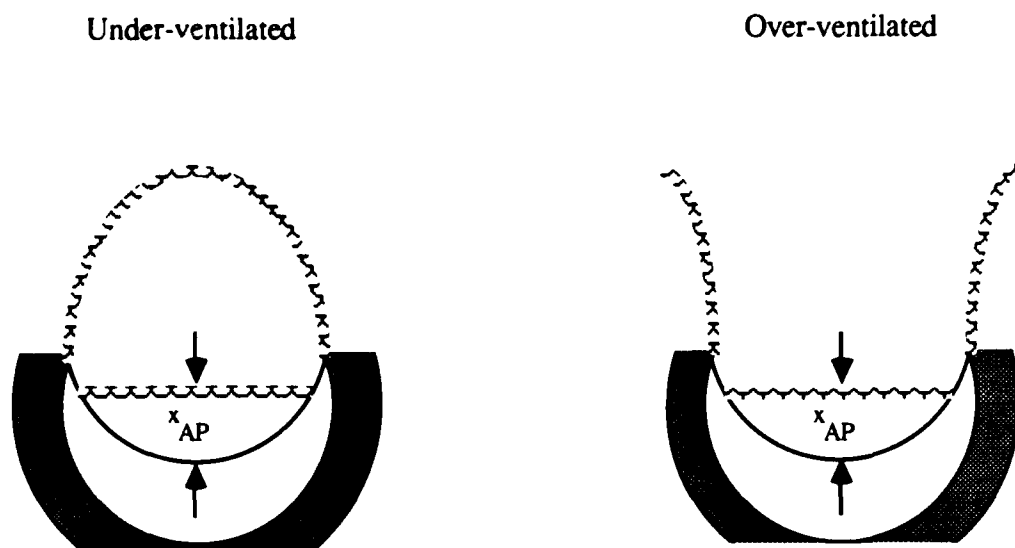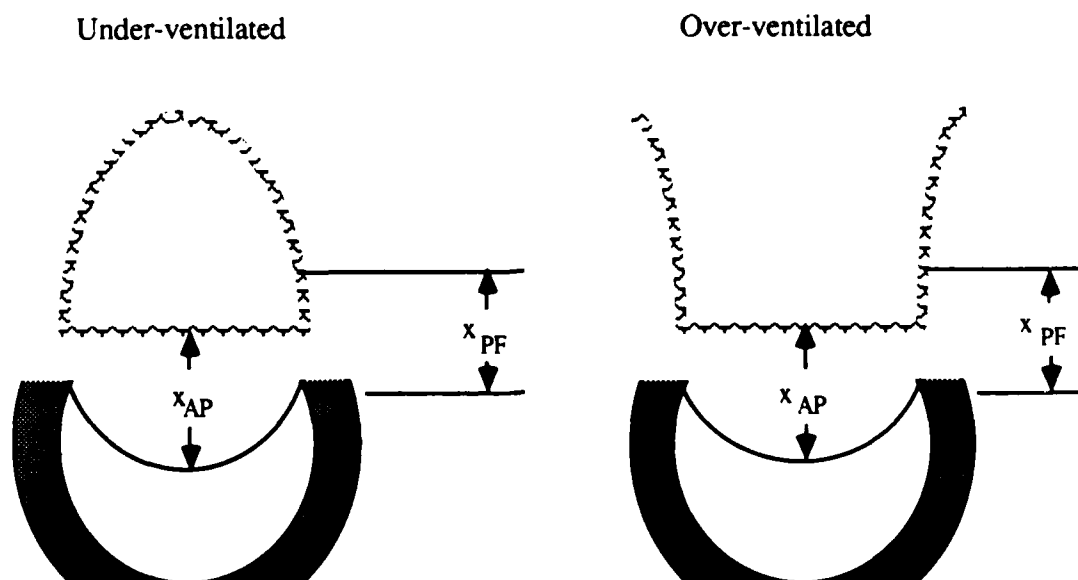
Under-ventilated

Over-ventilated

Figure 6. Case A

Under-ventilated

Over-ventilated

Figure 7. Case B

Figure 8. Case C

Figure 9. Case D

Under-ventilated   Over-ventilated
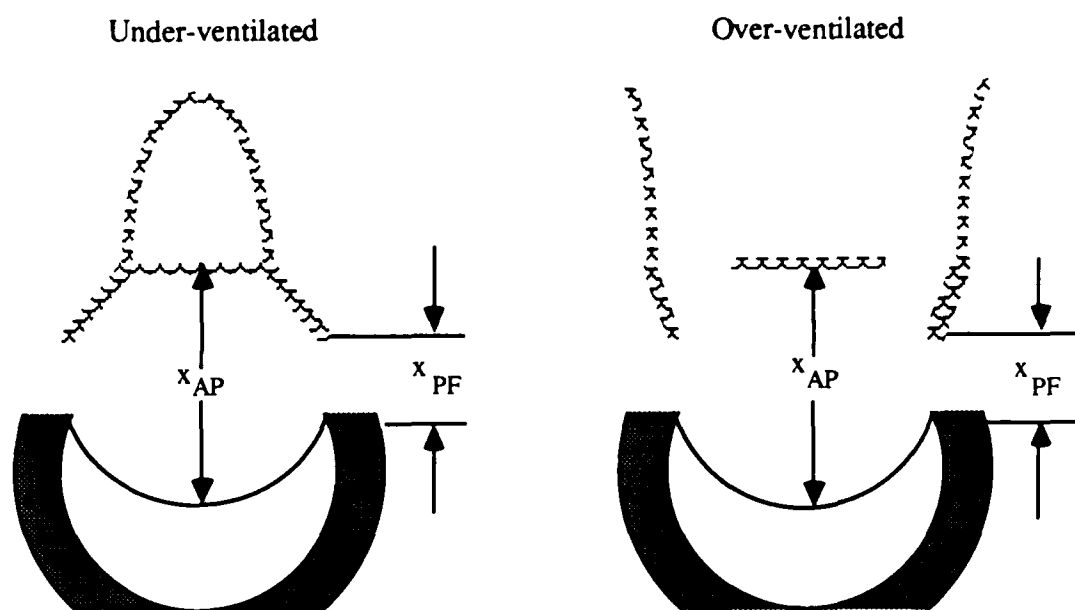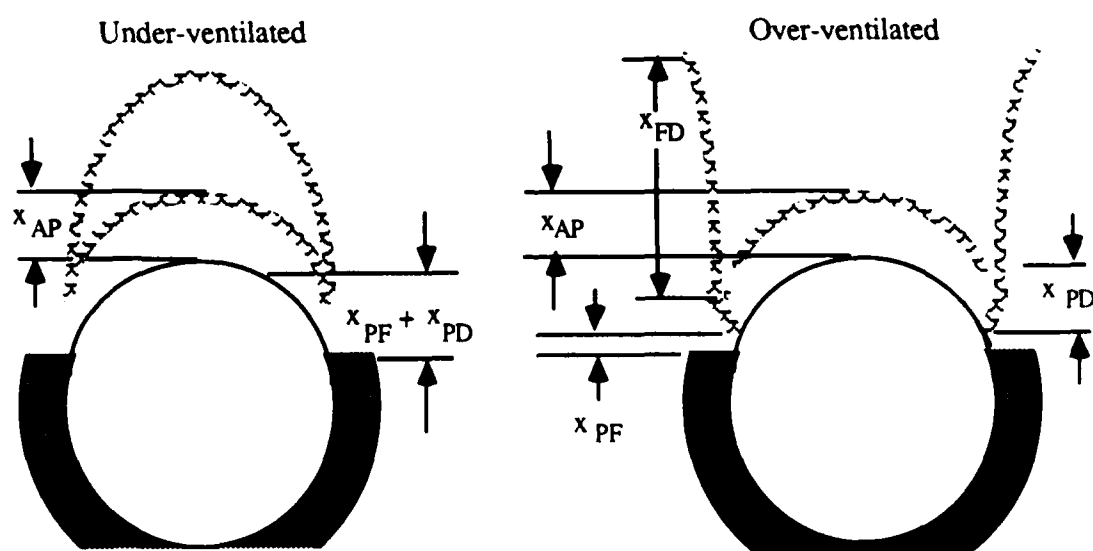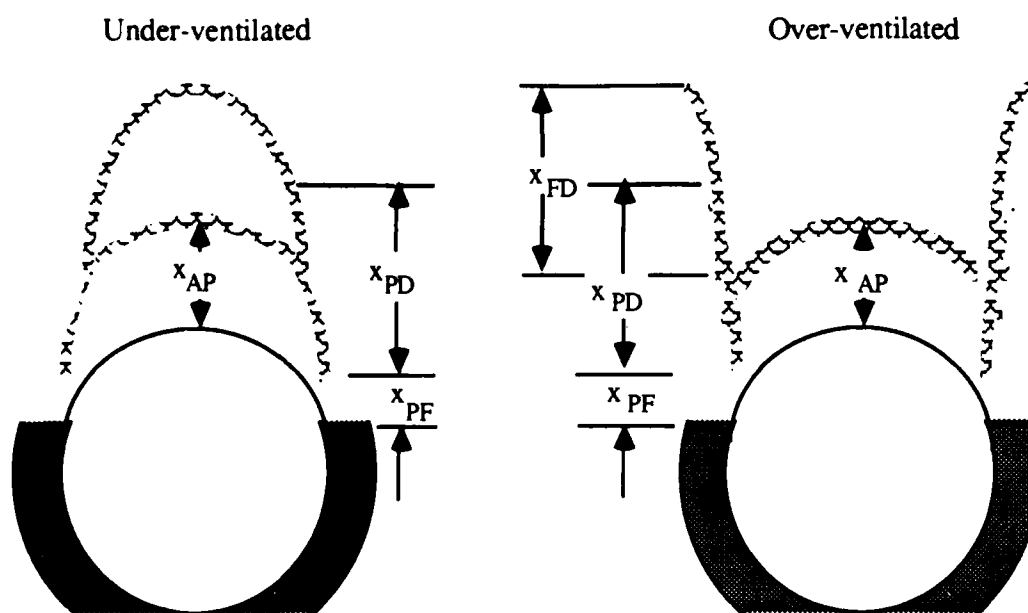

Figure 10. Case E

CHAPTER 4 - COMBUSTION MODEL VALIDATION AND RESULTS

In this chapter, results of steady state burning calculations for a series of polydisperse propellants using the COR model are compared with experimental data. Also, parametric studies have been performed on a series of monodisperse "computer" propellants; more specifically, propellants wherein the oxidizer particle size is arbitrarily assigned while total propellant properties are held fixed. These parametric studies are performed in order to analyze how oxidizer particle size affects the propellant's burning behavior when all other environmental factors are held constant. This study is deemed worthwhile since the COR model calculates the burning rate of a polydisperse, multimodal propellant based upon the burning responses of its individual, monodisperse pseudo-propellants. Finally, sample graphical output depicting the flame structure at discrete points in the regression of the propellant surface is presented. Such graphical depicting of the flames' structure is helpful if gaining a physical understanding of what processes are governing the burning rate at different points in the surface regression is desired.

4.1. Miller's Nonaluminized Propellant Series.

Before the burning rate calculations can be performed for a particular propellant, its formulation must be characterized for input into the COR model. More specifically, the particle size and size distribution for each oxidizer mode must be specified by means of the the two parameter, log-normal distribution function represented by Eq. (23). The two parameters in this distribution function are the fifty percent weight mean diameter, D_{ox}, and the mode width parameter, σ_{ox}. These parameters are determined for a particular oxidizer grind via a nonlinear regression analysis on actual grind distribution data. Such analysis provides the "best fit" values for D_{ox} and σ_{ox} for each oxidizer grind considered. In addition to the oxidizer grind distribution data, the mass fraction of each oxidizer mode must be specified along with data concerning the other propellant additives, whether they

be aluminum particles, catalysts, burning rate modifiers, etc. Finally, the type and amount of fuel binder must be specified.

In this section, data for a series of nonaluminized propellants which were provided by Hercules, Inc., as reported by Miller[10], are presented. The data presented are for a series of constant, 87.37 percent solids loaded, AP-based composite propellants. These propellants were formulated from up to four out of a possible eight AP grinds available. Table 1 gives the formulations for each of the propellants in the Miller series. For each propellant in Table 1, the fraction of the propellant made up of each of the eight possible oxidizer grinds is shown. The grinds are listed by a representative "as received" nominal diameter at the top of each column. Also shown on this table are the corresponding fifty percent weight mean diameter and mode width parameter for each of the eight possible oxidizer grinds. These propellants are primarily trimodal, in which case there are three separate values for D_{ox} and σ_{ox} along with a corresponding mass fraction required as input to the COR model. Table 1 also presents the experimentally determined burning rate and pressure exponent data given by Miller. These data have been obtained at a combustion pressure of 6.89 MPa and an initial solid propellant temperature of 294 K.

4.2. Propellant Constants Determination.

Within the equations comprising the COR model described previously, the adiabatic flame temperature for the diffusion flames and the AP monopropellant flame need to be specified along with the respective molecular weights of the combustion products of these flames. These flame parameters are important in determining heat transfer characteristics of the various flame zones and also in determining the velocity of the gases leaving the propellant surface. From a thermodynamic point of view, these two flame parameters are functions of both the combustion gas pressure and the initial reactant temperature, and more importantly, the propellant formulation. The percent of oxidizer plays an important role in

Table 1. Propellant Formulations: Nonaluminized Miller Propellant Series

Propellant Designation SD-III-88-		$400\,\mu$ $448.\,\mu$ 1.222	$200\,\mu$ $195.\mu$ 1.628	$90\,\mu$ $71.0\,\mu$ 1.370	$50\,\mu$ $44.2\,\mu$ 1.445	$20\,\mu$ $22.6\,\mu$ 1.676
	D_{ox} σ_{ox}					
01		-	-	-	-	.4526
02		-	-	.3158	-	.1386
03		-	-	-	-	.5579
04		-	.3158	-	-	.2421
05		.4211	-	-	-	.1368
06		-	-	-	.3158	.1368
07		-	-	.3158	-	.1368
08		-	-	-	.3158	.2421
09		-	.3158	-	-	.2421
10		.4211	-	-	-	.1368
11		-	-	-	-	.4526
12		-	-	-	-	.5579
13		-	-	-	-	.5579
i4		-	.3158	-	-	.2421
15		.4211	-	-	-	.1368
16		-	.3158	-	.3158	.2421
17		-	-	.3158	-	.5579
18		-	-	.4211	-	.4526
19		-	.3158	-	-	.5579
20		.4211	-	-	-	.4526
21		.3158	.3158	-	.1053	.1368
22		.3158	-	-	.4211	.1368
23		-	.4211	-	.3158	.1368
24		-	.3158	-	.4211	.1368
25		.4211	-	-	.3158	.1368

Table 1. (continued)

Propellant Designation SD-III-88-	D_{ox} / σ_{ox}	6 μ 5.23 μ 1.878	2 μ 1.89 μ 1.305	.7 μ .686 μ 2.716	$r_{6.89}$ (mm/s)	$n_{6.89}$
01		.3158	-	.1053	-	-
02		-	-	.4211	29.77	.916
03		-	-	.3158	36.30	.689
04		-	-	.3158	28.47	.797
05		-	-	.3158	22.53	.928
06		.3158	.1053	-	29.03	.612
07		-	.4211	-	-	-
08		-	.3158	-	27.86	.692
09		-	.3158	-	27.43	.771
10		-	.3158	-	22.78	.841
11		.4211	-	-	-	-
12		.3158	-	-	22.26	.617
13		.3158	-	-	-	-
14		.3158	-	-	24.77	.613
15		.3158	-	-	18.24	.690
16		-	-	-	14.17	.451
17		-	-	-	21.18	.474
18		-	-	-	18.03	.437
19		-	-	-	19.74	.529
20		-	-	-	14.17	.610
21		-	-	-	8.28	.430
22		-	-	-	13.16	.458
23		-	-	-	11.71	.463
24		-	-	-	13.64	.449
25		-	-	-	11.20	.528

determining these parameters, as do the amount and types of additives incorporated into the propellant formulation, when additives are present.

In the COR model, as discussed in Chapter 3, the oxidizer surface is allowed to regress at a different rate from that of the fuel surface, so, in general, at any arbitrary burning increment, the percent of oxidizer burning with the fuel will not be the same as the percent of oxidizer in the overall propellant. The adiabatic flame temperature for the primary and final diffusion flames will therefore change with each incremental burning calculation made. Once the instantaneous oxidizer to fuel ratio is determined in the COR model, the NASA Themochemistry Program[11] is used to determine the primary and final flame temperature. The temperature of the AP flame only needs to be calculated once, however, since in this flame the AP is only burning with itself. In all cases, the AP monopropellant flame temperature is approximately 1406 K at 6.89 MPa.

For all cases considered, the molecular weight of the AP flame is 27.9 kg/kmole, and the primary and final flames' molecular weight is determined to be 25.7 kg/kmole. The molecular weight of the primary and final flames was calculated assuming that the oxidizer mass ratio is the same as that of the overall propellant. While this assumption contradicts the assumption just made regarding the flame temperature of the primary and final flames, the correction of the molecular weight to reflect the instantaneous oxidizer/fuel mass ratio would be slight, and the approximation of a constant value is considered to be acceptable. In all cases, the values calculated for the molecular weights and adiabatic flame temperatures were made assuming a combustion pressure of 6.89 MPa and an initial solid propellant temperature of 294 K.

As in the case with other steady-state burning rate models, the COR model requires the use of several input constants such as the activation energies and the pre-exponential frequency factors for the many chemical reactions considered, the heats of fuel pyrolysis and oxidizer decomposition, and the specific heats and thermal conductivities for both the gas and solid phases. Some of these constants are known only to a small degree of

precision. Many of these parameters can be obtained from various references throughout the literature. For example, Reference 12 lists the experimentally obtained values of the heat of decomposition, the density, pyrolysis constants, and the stoichiometric variables for HTPB, the fuel binder used in the Miller propellants being considered here. Ammonium perchlorate (AP) constants can be obtained from available literature dealing with AP monopropellant decomposition studies[13]. However, other parameters can only be estimated, and for this task, experimental burning rate and pressure exponent data for the propellant formulations investigated can be used. For the Miller formulations considered here, the experimentally determined burning rates and pressure exponents for the formulations at 6.89 MPa and an initial solid propellant temperature of 294 K are shown in Table 1. Using the COR model, the theoretical burning rate and pressure exponent for each Miller formulation have been calculated and compared with the experimental values. In this manner, some of the lesser-known numerical input constants can be varied, each within prescribed limits, until the best fit to the experimental data, both for burning rate and pressure exponent, is obtained.

The results of this theoretical versus experimental burning rate and pressure exponent comparison is presented in Tables 2 and 3. Table 2 presents the comparison between experiment and theory for the burning rate at 6.89 MPa, and Table 3 presents the comparison between experiment and theory for the pressure exponent at 6.89 MPa. In each of these tables, the percent error between theoretical and experimental values is listed. The average error for the burning rate comparison is approximately 12 percent, whereas the average percent error for the pressure exponent comparison is about 20 percent. The greatest disparity is found to occur for formulations which contain high percentages of intermediate-sized oxidizer grinds (5.23 μm – 22.6 μm).

Renie[6] performed an identical experimental versus theoretical comparison on the burning rate and pressure exponent data of Miller's formulations described herein using the PEM, which is the model modified in developing the COR model. The reported results of

Table 2. Experimental Versus Theoretical Burning Rate Comparison

Propellant Number SD-III-88-	Rate-theo. (mm/sec)	Rate-expr. (mm/sec)	Error (Percent)
01	25.73	-	-
02	30.20	29.77	1.45
03	28.80	36.30	-20.65
04	25.61	28.47	-10.03
05	23.03	22.53	2.23
06	24.32	29.03	-16.24
07	28.74	-	-
08	26.66	27.86	-4.31
09	24.52	27.43	-10.62
10	21.93	22.78	-3.71
11	23.65	-	-
12	20.25	26.26	-22.88
13	22.58	-	-
14	19.39	24.77	-21.71
15	16.81	18.24	-7.84
16	15.13	14.17	6.78
17	17.62	21.18	-16.82
18	17.03	18.03	-5.52
19	16.18	19.74	-18.05
20	13.59	14.05	-4.07
21	11.50	8.26	38.89
22	13.64	13.16	3.67
23	14.07	11.71	20.13
24	14.78	13.64	8.37
25	12.55	11.20	12.04

Table 3. Experimental Versus Theoretical Pressure Exponent Comparison

Propellant Number SD-III-88-	n-theo.	n-expr.	Error (Percent)
01	.590	-	-
02	.710	.916	-22.47
03	.706	.689	2.48
04	.684	.797	-14.22
05	.675	.928	-27.30
06	.516	.612	-15.69
07	.512	-	-
08	.538	.692	-22.25
09	.508	.771	-34.05
10	.478	.841	-43.11
11	.531	-	-
12	.511	.617	-17.24
13	.552	-	-
14	.497	.613	-18.86
15	.456	.690	-33.86
16	.558	.451	23.69
17	.603	.474	27.16
18	.592	.437	35.49
19	.581	.529	9.74
20	.546	.610	-10.55
21	.476	.430	10.70
22	.539	.458	17.64
23	.533	.463	15.12
24	.550	.449	22.40
25	.515	.528	2.39

the PEM comparison was somewhat closer to Miller's experimental values both for the burning rate and pressure exponent; however, as will be shown below, the oxidizer particle size dependency of the burning rate phenomenon is much more complex when the continuous oxidizer regression behavior incorporated in the COR model is taken into account. Therefore, finding a good fit of input constants to experimental data becomes a more complicated task.

4.3. Parametric Studies.

Having established the numerical value of the many constants necessary as input to the COR model, theoretical calculations can now be performed. In this section, the steady state burning response of a series of monodisperse "computer" propellants, or pseudo-propellants, is presented. That is, the propellant formulations under consideration are identical with the only parameter varying being the size of the oxidizer particle. In this manner, the effects that oxidizer particle size have on the calculated steady state burning response can be determined.

For this study, the "computer" propellants under consideration are taken to be unimodal and comprised of 87.37 percent by weight ammonium perchlorate (AP) oxidizer and 12.63 percent HTPB fuel binder. For each calculation, the initial solid propellant temperature is assumed to be equal to 294 K. Calculations are made for burning rate and pressure exponent at a single combustion pressure of 6.89 MPa. Figures 11 and 12 present the steady state burning rate, r, and pressure exponent, n, respectively, for each "computer" propellant, or pseudo-propellant. The oxidizer particle size has been varied from fine (1 μm) to very coarse (1000 μm). The burning rate results of Fig. 11 follow the characteristic S-shaped profiles which have been experimentally observed. That is, small oxidizer propellants burn extremely fast, while coarser oxidizer propellants burn at an increasingly slower rate. Examining the pressure exponent results of Fig. 12, it is evident that the smaller oxidizer propellants burn with an increased pressure exponent, while
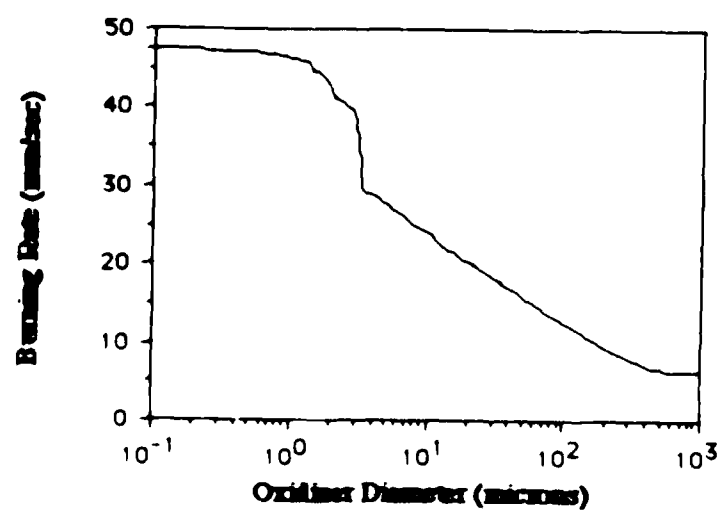
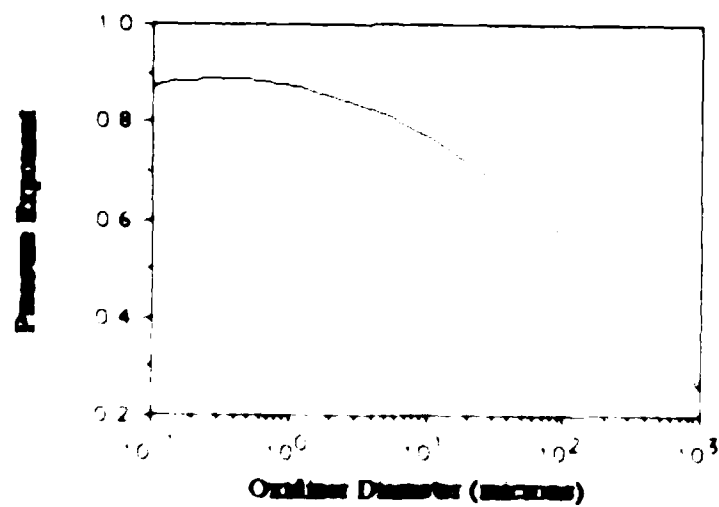Figure 11. Pseudo-propellant Burning Rate Results

Figure 12. Pseudo-propellant Pressure Exponent Results

while decreasing the oxidizer particle size within the propellant formulation tends to decrease the calculated value of pressure exponent.

The characteristics observed in these two figures can be explained on the basis of specific flame dependencies. Within the COR model, the heat transfer to the propellant surface and thus the propellant burning rate and value of the surface temperature is calculated from a summation of the heat transfer from each of the three flames surrounding the oxidizer particle at the propellant surface. For different sized oxidizer particles, different flames dominate the heat transfer to the surface. Smaller oxidizer particle pseudo-propellants are controlled by the primary kinetic flame which tends to yield high burning rates. Also, the pressure exponent values are high due to the high reaction order assigned to this flame. As the oxidizer particle size increases, all three flames contribute to the overall burning rate of the propellant, thus resulting in a significant lowering in both the burning rate and the pressure exponent. Finally, as the oxidizer particle size is further increased, the AP monopropellant flame gains dominance causing the pressure exponent to continue to decrease and the burning rate to further decrease with corresponding decreases in both the propellant surface temperature, T_s, and the heat flux back to the surface. A similar discussion of the oxidizer particle size dependency on the value of burning rate and pressure exponent as calculated with the original PEM is contained in Renie[6]. However, in the PEM results[6], the pressure exponent began to increase for the large oxidizer as the AP flame came into dominance. Also, the burning rate variation with oxidizer diameter was found to have a much smoother transition from high burning rate to low burning rate.

The above remarks regarding the flame formation dependency on oxidizer particle size are in general correct. However, in the COR model, where the oxidizer surface and fuel surfaces are continuously regressing, and, in general, regressing at different rates, the oxidizer/fuel mass ratio can vary greatly during the burning of a single particle. Hence while a given particle size pseudo-propellant is dominated by the formation of certain flames, as the surface regresses, the flame formation processes can go through an

evolutionary process, where at different time intervals, different flames will form above the surface. Also, the interplay between surface geometry and flame formation, as discussed in Chapter 3, leads to a more "on-off" nature of which flames exist at any given burning interval. These points are discussed further in the next section. Such behavior has caused the obvious discrepancies between the pressure exponent and the burning rate results presented herein and those discussed in Renie[6].

4.4. Typical Time-Dependent Oxidizer Regression.

As described in Chapter 3, in the analysis of the burning process of a single oxidizer/fuel binder pair, the COR model assumes continuously regressing fuel and oxidizer surfaces. In this light, at discreet time increments during the surface regression, the model will calculate an instantaneous surface temperature and corresponding surface burning rate. Based on these discreet values of surface burning rate, the time it takes for the propellant to regress from one planar surface to the next can be determined, and the total time it takes for either the oxidizer or the fuel to be completely consumed is used to calculate a burning rate for the propellant.

The COR model has been adapted to run on a Macintosh Plus computer, and using the graphics capabilities of the Macintosh, it is possible to draw a "picture" of the burning propellant surface and the flames forming above an individual oxidizer particle at discrete time intervals during the burning process. This graphical technique aids in getting a feel for what physical processes are underway at any particular point in the surface regression scenario.

A representative sample series of graphical output which can be obtained is provided in Fig. 13. The pseudo-propellant oxidizer diameter chosen for display was 2 microns, with an initial propellant temperature of 294 K and a combustion pressure of 6.89 MPa. In each "screen" the incremental slice number is provided. Combustion data included for display are the instantaneous surface temperature, oxidizer mass fraction, and

burning time increment, along with the depiction of the flame structure corresponding to each state represented. The scaling factor used for drawing the flame structure on the "screen" is also provided. This oxidizer diameter has been chosen to show the competing nature of the three flames as the oxidizer is consumed.

As the oxidizer first begins to be exposed to the surface, the oxidizer to fuel mass ratio is very low, and the flames formed will be an AP flame just above the concave oxidizer surface and a final diffusion flame above the planar suface. As the oxidizer surface continues to regress faster than the fuel surface, the oxidizer to fuel mass ratio increases, and hence, the flame and surface temperatures increase as well. Eventually, a primary flame is allowed to form. However, at the same time, the center of the oxidizer surface continues to lie deeper and deeper below the fuel surface, until the AP flame can only form below the planar surface, eliminating the possibility for the formation of the primary diffusion flame. Also, it can be seen that as the oxidizer surface becomes more and more nonplanar, the mass flux from this surface increases, eventually leading to the formation of an over-ventilated diffusion flame. This increase in the oxidizer mass flux also eventually makes the oxidizer to fuel mass ratio exceed the stoichiometric value, leading to a lower value for the final diffusion flame temperature and consequently also a lower surface temperature.

```
FLAME SCALE : 1.000
 INCREMENT NUMBER :   1
SURFACE TEMP : 1147.0 K
ALPHA :  .3519
DT : 11.58000 SEC(10**-6)
```
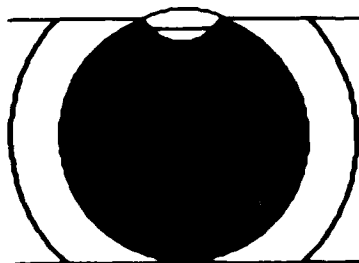
```
FLAME SCALE : 1.000
 INCREMENT NUMBER    2
SURFACE TEMP  1177.0 K
ALPHA   6427
DT   5.35200 SEC(10**-6)
```
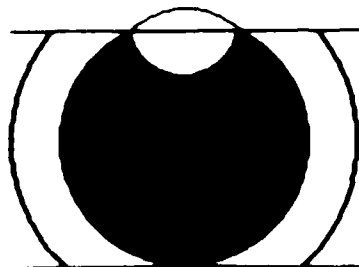
```
FLAME SCALE  1.000
 INCREMENT NUMBER    3
SURFACE TEMP  1252.0 K
ALPHA   7753
DT   4.12600 SEC(10**-6)
```
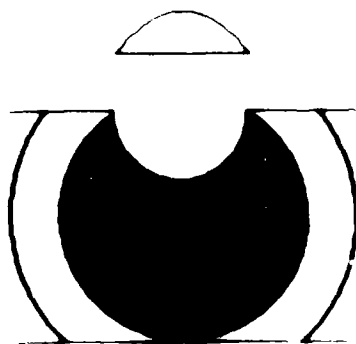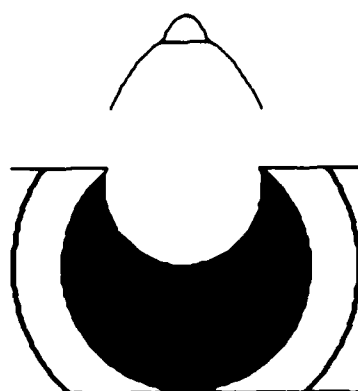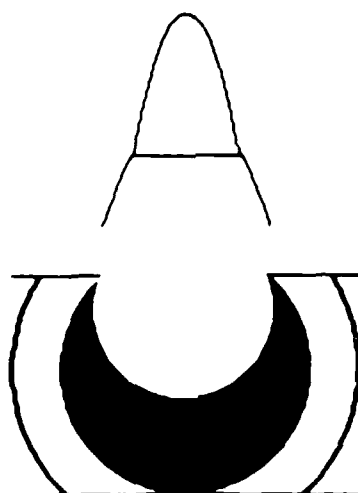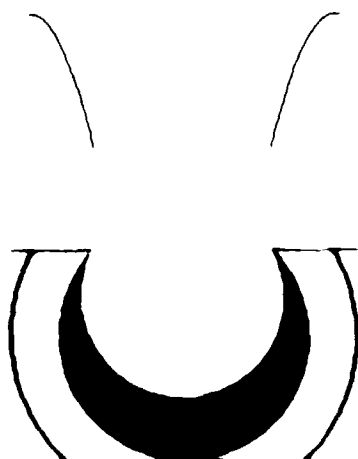
Figure 13 Sample Graphical Output Two Micron Particle

60


```
FLAME SCALE:1.000
INCREMENT NUMBER:   4
SURFACE TEMP:1264.0 K
ALPHA:.8467
DT:  3.43300 SEC(10**-6)
```



```
FLAME SCALE:1.000
INCREMENT NUMBER:   5
SURFACE TEMP:1206.0 K
ALPHA:.8857
DT:  3.78100 SEC(10**-6)
```



```
FLAME SCALE 1.000
INCREMENT NUMBER   6
SURFACE TEMP 1269 0 K
ALPHA  9120
DT   3 74100 SEC(10**-6)
```

Figure 13. (Continued)

```
FLAME SCALE:1.000
 INCREMENT NUMBER:   7
SURFACE TEMP:1045.0 K
ALPHA:.9282
DT: 4.98800 SEC(10**-6)
```
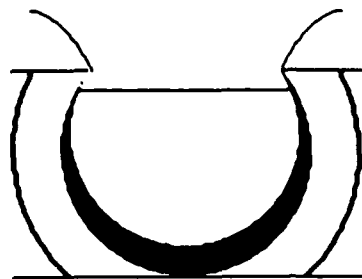
```
FLAME SCALE:1.000
 INCREMENT NUMBER:   8
SURFACE TEMP:1018.0 K
ALPHA:.9293
DT:11.23000 SEC(10**-6)
```
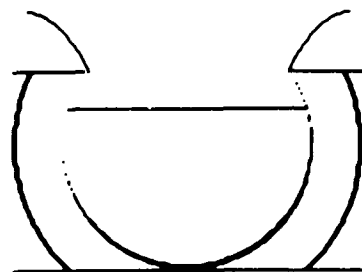
```
FLAME SCALE:1.000
 INCREMENT NUMBER:   9
SURFACE TEMP:1010.0 K
ALPHA:.9332
DT:   .90290 SEC(10**-6)
```
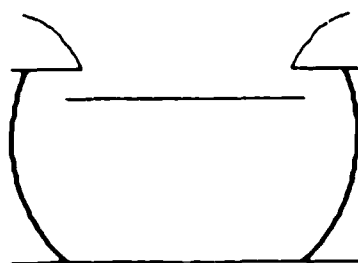
Figure 13 (Continued)

CHAPTER 5 - CONCLUSIONS

In the previous chapters, earlier composite solid propellant combustion models have been discussed, and the significant differences between these models and the proposed Continuous Oxidizer Regression (COR) model have been discussed as well. An experimental validation of the COR model has also been performed. Results from the experimental validation of the COR model show that the model does, in general, correctly predict trends regarding both the burning rate and pressure exponent of actual solid propellants. It has been shown that the predictions of the COR model, however, do not agree with experimental results as closely as do the predictions of the earlier multiple flame-based PEM model, which has been modified in the development of the COR model.

The souces for the differences between the COR and PEM predictions have been discussed. Notably, due to the continously regressing nature of the propellant surface in the COR model, different flames dominate the burning of the oxidizer/fuel pair pseudo-propellant at different points in the surface regression. This fact makes it more difficult to obtain a good fit of theoretical predictions to experimental predictions than in the case of the PEM model, where only one set of flames dominates the burning rate of a particular oxidizer particle size, due to the time-averaged nature of this model. Also, the geometric assumptions of the COR model lead to greater restrictions regarding the formation of the primary diffusion flame, further complicating the process of fitting theoretical predictions to experimental results.

The Macintosh-based graphical output of the COR model provided has shown this model's utility in gaining a better understanding of the physical processes governing the formation of different flames during different points in the regression of the fuel surface. While the predictive capabilities of the COR model are presently not as accurate as other models, the utility of this model in gaining a better overall understanding of the physical processes governing solid propellant combustion has been demonstrated.

REFERENCES

1. Summerfield, M., Sutherland, G.S., Webb, M.J., Taback, H.J., and Hall, K.P., "Burning Mechanism of Ammonium Perchlorate Propellants," *ARS Progress in Astronautics and Rocketry - Vol. 1: Solid Propellant Rocket Research*, Academic Press, New York, 1960, pp. 141-182.

2. Ramohalli, K.N.R., "Steady-State Burning of Composite Propellants under Zero Cross-Flow Situation," *Fundamentals of Solid-Propellant Combustion - Progress in Astronautics and Aeronautics: Volume 90*, Edited by K. Kuo and M. Summerfield, 1984, pp. 409-477.

3. Hermance, C.E., "A Model of Composite Propellant Combustion Including Surface Heterogeneity and Heat Generation," *AIAA Journal*, Vol. 4, No. 9, September 1966, pp. 1629-1637.

4. Beckstead, M.W., Derr, R.L., and Price, C.F., "A Model of Composite Solid Propellant Combustion Based on Multiple Flames," *AIAA Journal*, Vol. 8, No. 12, December 1970, pp. 2200-2207.

5. Burke, S.P. and Schumann, T.E.W., "Diffusion Flames," *Industrial and Engineering Chemistry*, Vol. 20, No. 10, October 1928, pp. 998-1004.

6. Renie, J.P., "Combustion Modeling of Composite Solid Propellants," PhD. Thesis, Purdue University, West Lafayette, Indiana, December 1982.

7. Glick, R.L., "On Statistical Analysis of Composite Solid Propellant Combustion," *AIAA Journal*, Vol. 12, No. 3, March 1974, pp. 384-385, also "Composite Propellant Combustion Modeling," unpublished work.

8. King, M.K., "Model for Steady State Combustion of Unimodal Composite Solid Propellants," AIAA Paper No. 78-216, AIAA 16th Aerospace Sciences Meeting, Huntsville, Alabama, January 1978.

9. King, M.K., "A Model of the Effects of Pressure and Crossflow Velocity on Composite Propellant Burning Rate," AIAA Paper No. 79-1171, AIAA/SAE/ASME 15th Joint Propulsion Conference, Las Vegas, Nevada, June 1979.

10. Miller, R.R., Donohue, M.T., Yount, R.A., and Martin, J.R., "Control of Solids Distribution in HTPB Propellants," AFRPL-TR-78-14, April 1978.

11. Gordon, S. and McBride, B.J., "Computer Program for Calculation of Complex Chemical Equilibrium Compositions, Rocket Performance, Incident and Reflected Shocks, and Chapman-Jouquet Detonation," NASA-SP-273, 1971.

12. Cohen, N.S., Fleming, R.W., and Derr, R.L., "Role of Binders in Solid Propellant Combustion," *AIAA Journal*, Vol. 12, No. 2, February 1974, pp. 212-218.

13. Price, C.F., Boggs, T.L., and Derr, R.L., "The Steady-State Combustion Behavior of Ammonium Perchlorate and HMX," AIAA Paper No. 79-0164, 17th Aerospace Sciences Meeting, New Orleans, Louisiana, January 1979.

APPENDIX A. GEOMETRIC CONSIDERATIONS

The following section covers geometric considerations which were included in developing the COR model. This appendix provides the necessary detail omitted during the discussion of the COR model in Chapter 3 above.

A.1. Fuel Diameter Calculation.

The oxidizer particle is assumed to be a sphere surrounded by the fuel binder. An average oxidizer diameter for each mode comprising a composite solid propellant, D_{ox}, is a parameter inputed into the COR model. Based upon these separate values of D_{ox}, the COR model then calculates diameters for each oxidizer/fuel binder pair or "pseudo-propellant" as referred to by the original PEM[6]. The following discussion involves calculations based upon a particular pseudo-propellant of diameter D_{ox}.

The first calculation needed is the calculation of the volume of fuel, V_f, which surrounds the oxidizer particle. An oxidizer mass fraction for each pseudo-propellant, α, is calculated by the COR model. This value of α is then modified as described in Chapter 3 to insure that after the fuel or oxidizer has been burned out, the burned reactants will have the required oxidizer/fuel mass ratio. The volume of the fuel can then be found from the formula

$$V_f = (1/\alpha - 1)\frac{\rho_{ox}V_{ox}}{\rho_f} \tag{A.1}$$

where ρ_{ox} and ρ_f are the densities of the oxidizer and the fuel, respectively, and V_{ox} is the oxidizer volume, found from the formula

$$V_{ox} = \frac{\pi}{6}D_{ox}^3 \tag{A.2}$$

Next, the geometry of the fuel surrounding the oxidizer needs to be evaluated. The oxidizer is always assumed to be a perfect sphere. There are two possible fuel geometries to be considered. In the first possible fuel geometry, the fuel consists of a sphere surrounding the oxidizer which is cut off at the top and bottom as show in Fig. A.1. (Note, in this and subsequent figures, the depiction of the fuel volume will be exagerated for the sake of clarity. In actuality, typical oxidizer/fuel mixtures would dictate smaller volumes of fuel.)
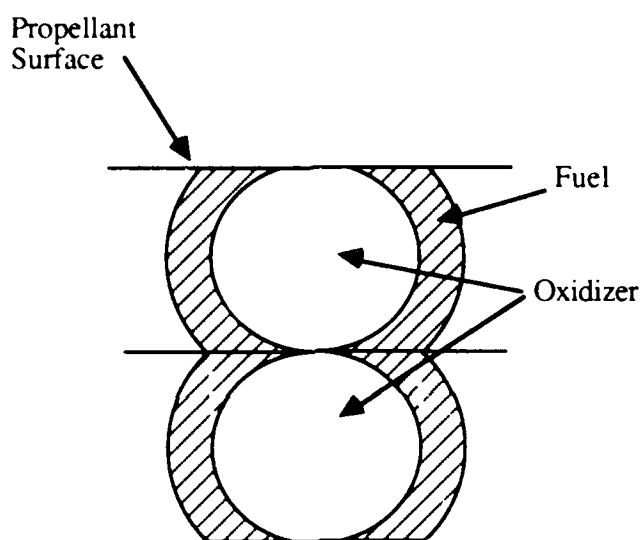
Figure A.1. Hypothetical Fuel-Oxidizer Geometry

To calculate of the diameter of a sphere of fuel clipped off at the points indicated in Fig. A.1 involves using the equation for the volume of a spherical cap,

$$V_{cap} = \frac{1}{3} h^2 (3r - h) \qquad (A.3)$$

where r is the radius of the sphere, and h is the height of the spherical cap, as shown Fig. A.2.
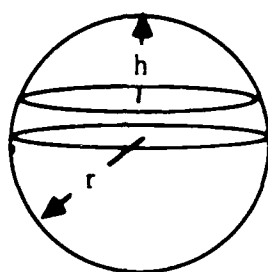
Figure A.2. Spherical Cap Nomenclature

With the equation for the spherical cap, and now referring to Fig A.3, the diameter of the fuel sphere surrounding the oxidizer sphere can be found.
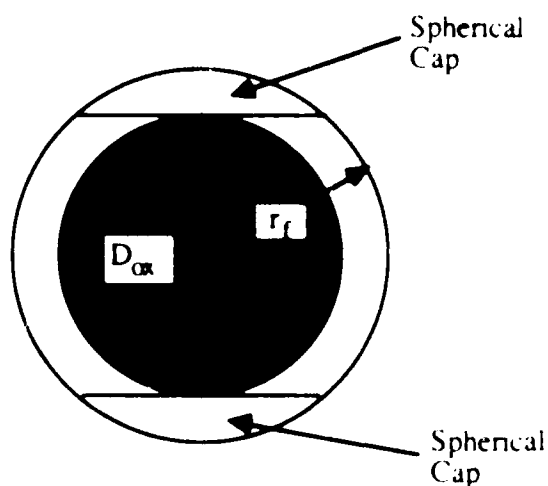
Figure A.3. Single Oxidizer/Fuel Geometry

The fuel volume V_f has already been given by Eq. (A.1); V_f is also equal to the following

$$V_f = V(r_f) - V_{ox} - 2V_{cap} \qquad (A.4)$$

The term $V(r_f)$ refers to the volume of a sphere of a given radius r_f. Substituting into Eq (A.4) for the values of $V(r_f)$ and V_{ox}, and also substituting the value of V_{cap} given by Eq. (A.3), V_f can be shown to be

$$V_f = \frac{3}{4}\pi\frac{D_{ox}^3}{8} - \frac{2}{3}\pi e^2(3r_f - e) \tag{A.5}$$

where e is the fuel binder annulus dimension and is given by

$$e = r_f - \frac{D_{ox}}{2} \tag{A.6}$$

Subsituting Eq. (A.6) into Eq. (A.5) yields the following expression for the volume of the fuel V_f

$$V_f = \frac{3}{4}\pi r_f^3 - \frac{\pi}{6}D_{ox}^3 - \frac{2}{3}\pi\left(r_f - \frac{D_{ox}}{2}\right)^2\left(3r_f - r_f + \frac{D_{ox}}{2}\right) \tag{A.7}$$

Through an expansion of terms, Eq. (A.7) can be simplified to

$$V_f = \pi D_{ox} r_f^2 - \pi\frac{D_{ox}^3}{4} \tag{A.8}$$

Rearranging Eq. (A.8), the following expression results

$$r_f^2 = \frac{1}{\pi D_{ox}}\left(V_f + \frac{D_{ox}^3}{4}\right) \tag{A.9}$$

The quantity V_f can be obtained from Eq. (A.1); therefore, the diameter of the fuel sphere surrounding an oxidizer particle of a given diameter D_{ox} is

$$D_f = 2\left[\frac{1}{\pi D_{ox}}\left(V_f + \frac{\pi D_{ox}^3}{4}\right)\right]^{1/2} \tag{A.10}$$

A.2. Height from Surface Calculation.

In treating the stepwise burning of a single oxidizer particle with surrounding fuel binder, it is necessary to partition the fuel or oxidizer into equal volumes. In order to perform calculations needed to determine the burning rate after each volume of fuel is consumed, it is necessary to know the height, h_f, of the planar fuel surface from the initial unburned surface, after each equal fuel volume is consumed.

Two different cases need to be considered for determining h_f. When working under the assumption that the fuel surrounds the oxidizer as a sphere cut off at the top and bottom, as shown in Fig. A.1, h_f can be calculated based upon the volume of fuel consumed. However, the fuel can also be assigned to the oxidizer such that at any arbitrary oxidizer surface, the propellant's overall fuel/oxidizer mass ratio is maintained. For this second case, it is easier to measure the height from the surface based upon the amount of oxidizer consumed. These two separate scenarios are discussed below.

A.2.1. Height Based on Fuel Regression.

For the case where the fuel is assumed to surround the oxidizer as a sphere cut off at the top and bottom, the total fuel volume is divided up into equal sub-volumes. As the COR model is formulated, a volume of the fuel is permitted to burn away, and the surface burning rate is then determined. Then another equal volume of fuel is burned, with the surface burning rate being determined once again. The height of the planar surface from the initial unburned surface must be determined each time, as shown in Fig. A.4.

In this representative figure, dV is an arbitrary volume of fuel which has been consumed. The parameter h_f is the incremental height from the surface at the time that dV amount of fuel has been consumed. The term dV is the volume of a spherical cap $(h_f + e)$ high minus the volume of a spherical cap e high and the volume of the oxidizer spherical cap h_f high, or in equation form

$$dV = \left[\frac{\pi}{3}(h_f + e)^2[3r_f - (h_f + e)]\right] - \left[\frac{\pi}{3}e^2(3r_f - e)\right] - \left[\frac{\pi}{3}h_f^2(3r_{ox} - h_f)\right] \quad (A.11)$$
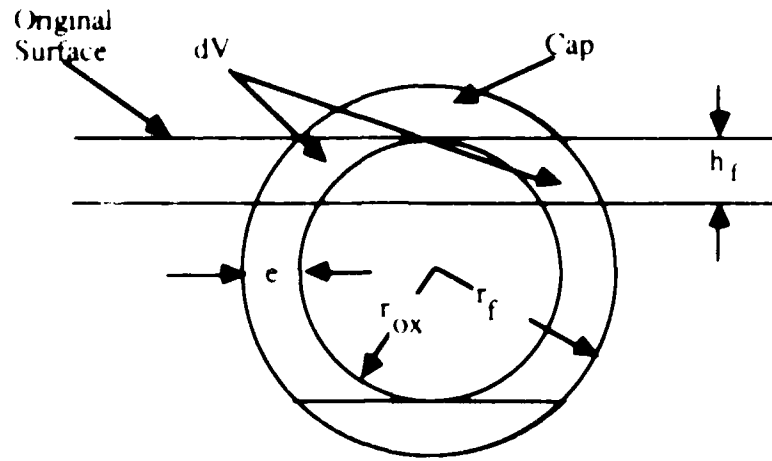

Figure A.4. Burning Oxidizer Particle

Factoring out the common term of $\pi/3$, Eq. (A.11) becomes

$$dV = \frac{\pi}{3}\left[\left[(h_f^2 + 2eh_f + e^2)(3r_f - h_f - e)\right] - e^2\left[3r_f - e\right] - h_f^2\left[3r_{ox} - h_f\right]\right] \quad (A.12)$$

which, upon expansion of terms, results in

$$dV = \frac{\pi}{3}\left[\begin{array}{c} 3r_f h_f^2 - h_f^3 - eh_f^2 + 6eh_f r_f - 2eh_f^2 - 2e^2 h_f + 3e^2 r_f \\[2mm] - e^2 h_f - e^3 - 3r_f e^2 + e^3 - 3r_{ox}h_f^2 + h_f^3 \end{array}\right] \quad (A.13)$$

Upon simplification Eq. (A.13) reduces to

$$dV = \frac{\pi}{3}\left[(3r_f - 3e - 3r_{ox})h_f^2 + 6er_f h_f - 3e^2 h_f\right] \quad (A.14)$$

Substituting for the value of $e = r_f - r_{ox}$ into Eq. (A.14), dV is found to be

$$dV = \frac{\pi}{3}\left[(0)h_f^3 + 6(r_f - r_{ox})r_f h_f - 3(r_f - r_{ox})^2 h_f \right]$$ (A.15)

which, upon further expansion of terms, becomes

$$dV = \frac{\pi}{3}\left[6r_f^2 h_f - 6r_{ox}r_f h_f - 3h_f\left[r_f^2 - 2r_f r_{ox} + r_{ox}^2 \right] \right]$$ (A.16)

which simplifies to the following

$$dV = \frac{\pi}{3}\left[3r_f^2 h_f - 3r_{ox}^2 h_f \right]$$ (A.17)

Rearranging Eq. (17), an expression for h_f in terms of dV and the known quantities r_{ox} and r_f is obtained

$$h_f = \frac{dV}{r_f^2 - r_{ox}^2}$$ (A.18)

If the fuel is divided into equal volumes, the the total volume dV of fuel burned at the end of any burning increment will simply be an integer multiple of what was burned in the first burning interval. Hence, after the kth burning interval the kth height from the surface calculated will simply be k times the height from the surface calculated after the first burning increment.

A.2.2. Height Based on Oxidizer Regression

In the stepwise burning of an oxidizer particle, the COR model has the option of calculating the burning rate for a given oxidizer particle size by assuming that at any height from the surface, the mass fraction of the fuel will be equal to the mass fraction of the fuel for the overall propellant. Since the fuel no longer assumes a spherical shape for this case, the height from the surface at which a given volume of fuel is burned is no longer obtainable as described in Sec. A.2.1 above. However, in this case, the volume of fuel consumed is directly proportional to the volume of oxidizer consumed. Hence, if heights from the surface are calculated based on equal volumes of oxidizer consumed, those heights will correspond to equal volumes of fuel consumed as well. The required nomenclature for the case where the height from the surface is based on the amount of oxidizer consumed is shown in Fig. A.5.
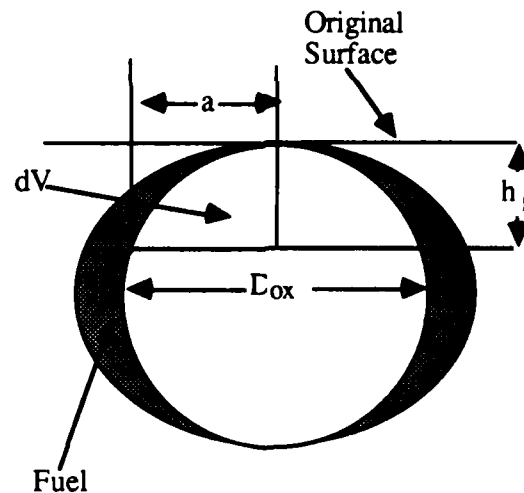
Figure A.5. Height Based Upon Oxidizer Consumed

The quantity dV is now an arbitrary volume of oxidizer which has been consumed. The quantity h_f is the height from the surface at the time that dV amount of oxidizer has been consumed. The quantity a is the radius of the oxidizer surface at the height h_f below the surface. The value of h_f needs to be solved for given the values of D_{ox} and dV.

From the equation for the volume of a spherical cap

$$dV = \frac{\pi}{3} h_f^2 \left(\frac{3}{2} D_{ox} - h_f \right)$$

(A.19)

and from trigonometry,

$$h_f = \frac{D_{ox}}{2} - \sqrt{\frac{D_{ox}^2}{4} - a^2}$$

(A.20)

Combining Eqs. (A.19) and (A.20), dV is found to be

$$dV = \frac{\pi}{3} \left[\frac{D_{ox}}{2} - \left[\frac{D_{ox}^2}{4} - a^2 \right]^{.5} \right]^2 \left[\frac{3}{2} D_{ox} - \left[\frac{D_{ox}}{2} - \left(\frac{D_{ox}^2}{4} - a^2 \right)^{.5} \right] \right]$$

(A.21)

After expanding and cancelling terms, Eq. (A.21) becomes

$$dV = \frac{\pi}{3} \left[\frac{D_{ox}^3}{4} - \left(a^2 + \frac{D_{ox}^2}{2} \right) \left(\frac{D_{ox}^2}{4} - a^2 \right)^{.5} \right]$$

(A.22)

which upon rearranging becomes

$$dV - \frac{D_{ox}^3}{16} = \frac{-\pi}{3} \left[\left(a^2 + \frac{D_{ox}^2}{2} \right) \left(\frac{D_{ox}^2}{4} - a^2 \right)^{.5} \right]$$

(A.23)

Further rearranging of terms results in

$$\left(a^2 + \frac{D_{ox}^2}{2}\right)\left(\frac{D_{ox}^2}{4} - a^2\right)^{?} = \frac{4}{\pi}\left(\frac{\pi}{16}D_{ox}^4 - dV\right) \qquad (A.24)$$

A new parameter V' is now defined in terms of the known quantities D_{ox} and dV as being equal to the expression on the right hand side of Eq. (A.24). Squaring both sides of Eq. (A.24) then results in

$$V'^2 = \left(a^2 + \frac{D_{ox}^2}{4}\right)^2\left(\frac{D_{ox}^2}{4} - a^2\right) \qquad (A.25)$$

which, after expanding and rearranging terms, becomes

$$V'^2 - \frac{D_{ox}^6}{16} = -a^6 - \frac{3}{4}D_{ox}^2 a^4 \qquad (A.26)$$

A second new parameter, V", is defined in terms of the known parmameters D_{ox} and V' as being equal to the expression on the left-hand side of Eq. (A.26). Then, if Eq. (A.26) is rearranged, a cubic equation for a^2 results

$$(a^2)^3 + \frac{3}{4}D_{ox}^2(a^2)^2 + V'' = 0 \qquad (A.27)$$

The standard solution of a cubic equation solves for the variable z in the equation

$$z^3 + c_1 z^2 + c_2 z + c_3 = 0 \qquad (A.28)$$

by assigning values to parameters Q and R of

$$Q = \frac{3c_2 - c_1^2}{9} \qquad (A.29)$$

and

$$R = \frac{9c_1 c_2 - 27c_3 - 2c_1^3}{54} \qquad (A.30)$$

For cubic equations such as Eq. (A.27), there are three possible solutions

$$z_1 = 2(-Q)^{.5}\cos(\frac{\theta}{3}) - \frac{c_1}{3} \qquad (A.31)$$

$$z_2 = 2(-Q)^{.5}\cos(\frac{\theta}{3} + \frac{2}{3}\pi) - \frac{c_1}{3} \qquad (A.32)$$

$$z_3 = 2(-Q)^{.5}\cos(\frac{\theta}{3} + \frac{4}{3}\pi) - \frac{c_1}{3} \qquad (A.33)$$

where θ is found from

$$\theta = \arccos\left[\frac{R}{(-Q)^{1/3}}\right] \qquad (A.34)$$

The particular values for Q and R in the solution to Eq. (A.27) are

$$Q = -\frac{D_{ox}^4}{16} \qquad (A.35)$$

and

$$R = \frac{V}{2} - \frac{D_{ox}^{6}}{64} \qquad (A.36)$$

The positive solution to Eq. (A.27) turns Eq. (A.31) into

$$a^2 = 2(-Q)^{.5} \cos(\frac{\theta}{3}) - \frac{D_{ox}^2}{4} \qquad (A.37)$$

From the geometry of a circle, it can be shown that

$$h_f = \frac{D_{ox}}{2} - \left[\frac{D_{ox}^2}{4} - a^2\right]^{.5} \qquad (A.38)$$

A.3. Surface Diameter Calculation.

Calculations involving the oxidizer/fuel stoichiometry and diffusion flame heights require a knowledge of the diameters of the fuel and the oxidizer at any given depth from the initial planar surface. While Eq. (A.37) can be used to determine the oxidizer surface diameter for any given volume of fuel burned away, it is not completely general since equal divisions of the fuel volume are not always considered. The following section describes how the oxidizer diameter can be found for cases where the fuel is divided up into equal volumes.

A.3.1. Oxidizer Diameter Calculation (Upper Hemisphere).

The nomenclature used in this section will be the same as that shown in Fig. A.5. The parameter h_f is calculated for some arbitrary volume of fuel, using methods already described. From the geometry of a circle, it can be seen that

$$\left(\frac{D_{ox}}{2} - h_f\right)^2 + a^2 = \frac{D_{ox}^2}{4} \qquad \text{(A.39)}$$

Since the oxidizer surface diameter d_{ox} is equal to $2a$, Eq. (A.39) can be rearranged to obtain

$$d_{ox} = 2\left[\frac{D_{ox}^2}{4} - \left(\frac{D_{ox}}{2} - h_f\right)^2\right]^{.5} \qquad \text{(A.40)}$$

A.3.2. Fuel Diameter (Upper Hemisphere).

The nomenclature for the fuel diameter calculation is shown in Fig. A.6. The case shown here is where the fuel surrounds the oxidizer as a sphere cut off at the top and bottom.

In this figure, D_{ox} is the overall oxidizer diameter and D_f is the fuel diameter calculated using Eq. (A.10). The parameter d_{ox} is an arbitrary oxidizer diameter at some distance from the surface, calculated using Eq. (A.40). The parameter d_f is the fuel diameter corresponding to the oxidizer diameter d_{ox}. The parameter r_{ox} is the radius of the oxidizer, and r_f is the radius of the fuel.

From trigonometry,

$$\frac{d_f}{2} = \left[r_f^2 - (r_{ox} - h_f)^2\right]^{.5} \qquad \text{(A.41)}$$

Also, from trigonometry,

$$r_{ox} - h_f = \left[r_{ox}^2 - \frac{d_{ox}^2}{4}\right]^{.5} \qquad \text{(A.42)}$$
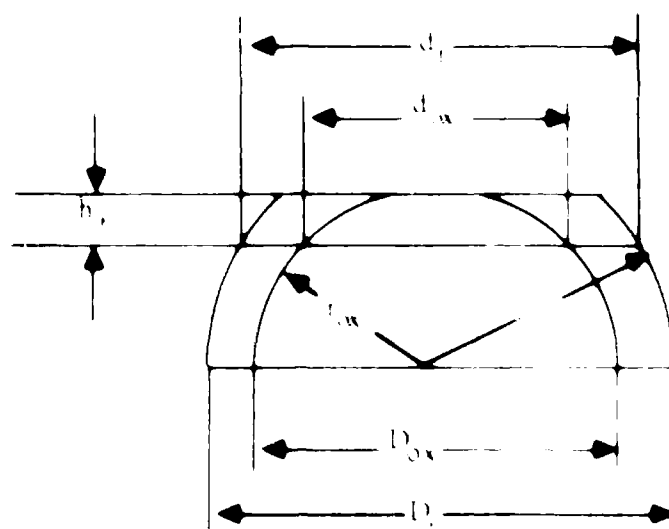
Figure A 6 Fuel Diameter Calculation Nomenclature

Substituting Eq. (A.42) into (A.41) yields

$$\frac{d_f}{2} = \left[r_f^2 - r_{ox}^2 - \frac{d_f^2}{4} \right]$$

In terms of D_{ox} and D_f, Eq. (A.43) becomes

$$d_f = \left[D_f^2 - D_{ox}^2 - d_{ox}^2 \right]$$

    For the case where the fuel is apportioned to the oxidizer based upon the fuel to oxidizer mass ratio of the overall propellant, as described in Sec. A.2.2, the fuel diameter at an arbitrary height from the surface is calculated in the following manner. The total density of the propellant, ρ_T is needed, which can be shown to be equal to

$$\rho_T = \frac{1}{(1-\alpha)/\rho_f + \alpha/\rho_{ox}} \tag{A.45}$$

where ρ_f and ρ_{ox} are the densities of the fuel and oxidizer, respectively, and α is the oxidizer mass fraction.

It can be shown that the volume fraction of the oxidizer, ζ_{ox}, is given by

$$\zeta_{ox} = \frac{\alpha\rho_T}{\rho_{ox}} \tag{A.46}$$

It follows directly then that d_f is given by

$$d_f = \frac{d_{ox}}{\sqrt{\zeta_{ox}}} \tag{A.47}$$

where d_{ox} can be found as described in Sec. A.2.2.

A.3.3. Lower Hemisphere Calculations.

All calculations shown so far have been derived in terms of the upper hemisphere. Once upper hemisphere values are determined, lower hemisphere values are easily obtained. In the COR model, the fuel is considered to be divided into k equal volumes per hemisphere. This translates into needing to calculate 2k-1 different values of d_f, d_{ox}, and h_f at 2k-1 different heights from the surface. The first k values can be calculated by the methods described above. The final k-1 values are obtained by noting

$$d_f(2k-i) = d_f(i) \tag{A.48}$$

$$d_{ox}(2k\text{-}i) = d_{ox}(i) \qquad\qquad (A.49)$$

$$h_f(2k\text{-}i) = D_{ox} - h_f(i) \qquad\qquad (A.50)$$

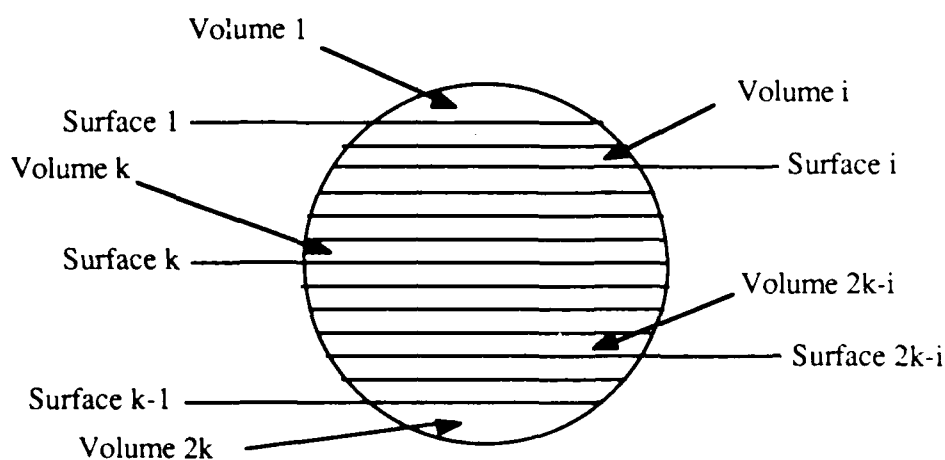The volume/surface nomenclature used in finding these lower hemisphere values is shown in Fig. A.7.

Figure A.7. Incremental Volume/Surface Nomenclature

A.4. Oxidizer Surface Geometry Calculations.

In general the fuel and oxidizer burn at different rates; hence, a flat burning surface is normally not maintained. In reality, the fuel surface will lie lower than the oxidizer surface, or the oxidizer surface will lie lower than the fuel surface, depending on which propellant species burns faster. In the COR model, the fuel surface is restricted to always regressing in a planar manner, with the oxidizer surface lying above or below the fuel surface. The oxidizer's burning is restricted in that its surface must remain continuous with the fuel surface. These two restrictions cause the oxidizer surface to be a spherical shape, either lying above or below the fuel surface, as shown in Figs. A.8 and A.9. Calculation

of the mass flux emanating from the oxidizer surface requires that the nonplanar oxidizer surface area be known.
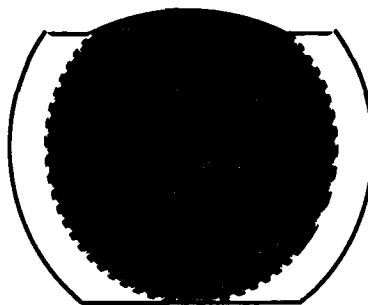

Figure A.8. Oxidizer Protruding Above Fuel Surface

Figure A.9. Oxidizer Recessed Below Fuel Surface

A.4.1. Concave Surfaces.

The first case to be investigated is the case where the oxidizer is burning faster than the fuel, forming a concave surface as shown in Fig. A.9. There are two possible scenarios associated with this case. The first possible scenario is where the depth of the oxidizer surface below the fuel surface is greater than the radius of curvature of the oxidizer surface. This condition is shown in Fig. A.10.
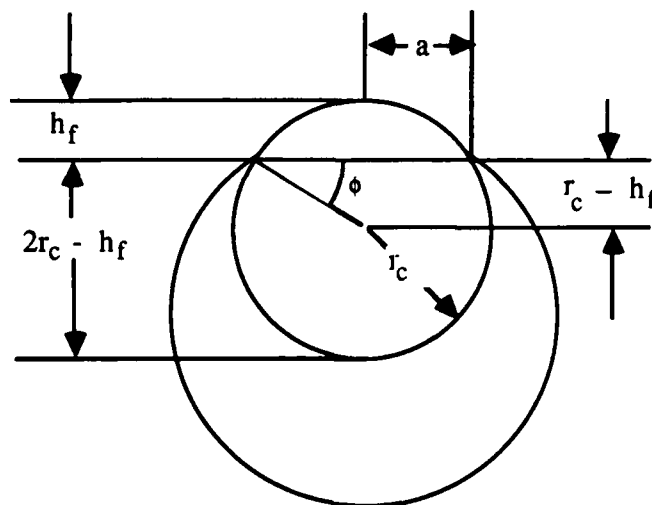
Figure A.10. Depth of Oxidizer Surface Greater than Surface Radius of Curvature

In this figure, r_c is the radius of curvature of the oxidizer surface and h_f is the height of the planar fuel surface below the original surface. The parmater a is the radius of the planar oxidizer surface at h_f below the original unburned surface. The values for a and h_f can be determined by methods already outlined.

From trigonometry,

$$r_c \sin\phi = r_c - h_f \qquad (A.51)$$

and

$$\cos\phi = \frac{a}{r_c} \qquad (A.52)$$

Now there are two equations and two unknowns, r_c and ϕ. To eliminate ϕ from the equations it is noted that the following are equivalent statements.

$$\cos\theta = u \qquad (A.53)$$

$$\sin\theta = \sqrt{1 - u^2} \qquad (A.54)$$

Applying this trigonometric identity to Eqs. (A.51) and (A.52) results in

$$r_c \left(1 - \frac{a^2}{r_c^2}\right)^{.5} = r_c - h_f \qquad (A.55)$$

The quantity $(2r_c - h_f)$ is the depth below the planar surface at which the lowest point of the oxidizer surface will lie. This quantity can be designated by h_{ox}, and is found by multiplying the time it takes the fuel to burn h_f by the burning rate of the oxidizer. When this quantity is substituted into Eq. (A.55), the following results

$$r_c \left(1 - \frac{a^2}{r_c^2}\right)^{.5} = h_{ox} - r_c \qquad (A.56)$$

This equation can be solved for r_c, resulting in

$$r_c = \frac{a}{2h_{ox}} + \frac{h_{ox}}{2} \qquad (A.57)$$

Or, in terms of d_{ox}, Eq. (A.57) becomes

$$r_c = \frac{d_{ox}}{h_{ox}} + \frac{h_{ox}}{2} \qquad (A.58)$$

With the value of r_c, it is possible to determine what the area of the nonplanar surface will be from the equation for the area of a spherical cap such as the one shown in Fig. A.2.

$$S_{ox} = 2\pi r_c h_{ox} \qquad (A.59)$$

The other possible configuration of a concave oxidizer surface is where the depth of the oxidizer is less than the radius of curvature of the surface, as shown in Fig. A.11.
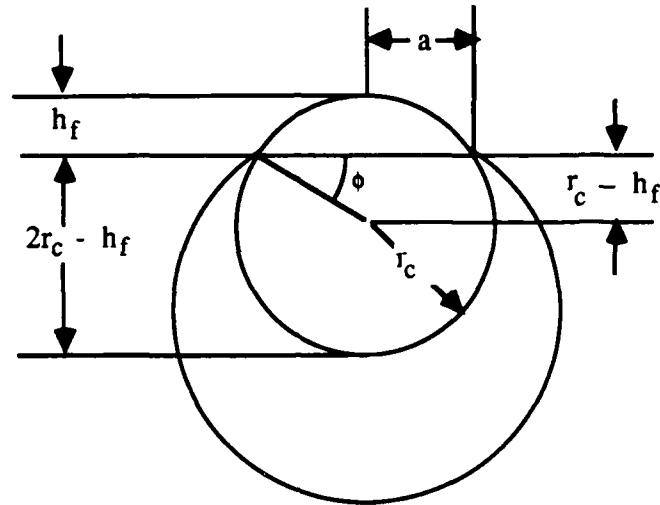
Figure A.11. Depth of Oxidizer Surface Less than Radius of Curvature

From trigonometry, it is clear that

$$r_c \sin\phi = r_c - h_{ox} \tag{A.60}$$

and

$$\cos\phi = \frac{a}{r_c} \tag{A.61}$$

Using the trigonometric identity of Eqs. (A.53) and (A.54) again results in

$$r_c^2 \left(1 - \frac{a}{r_c^2}\right)^{.5} = r_c - h_{ox} \tag{A.62}$$

which, when simplified, will yield the same value for r_c as that given in Eq. (A.58). The surface area is once again given by Eq. (A.59).

A.4.2. Convex Surfaces.

For the case where the oxidizer burns slower than the fuel, there are again two possible scenarios. The first scenario to be considered is where the oxidizer's height above the surface is greater than the oxidizer surface's radius of curvature. This condition is shown in an exagerated form in Fig. A.12. below.
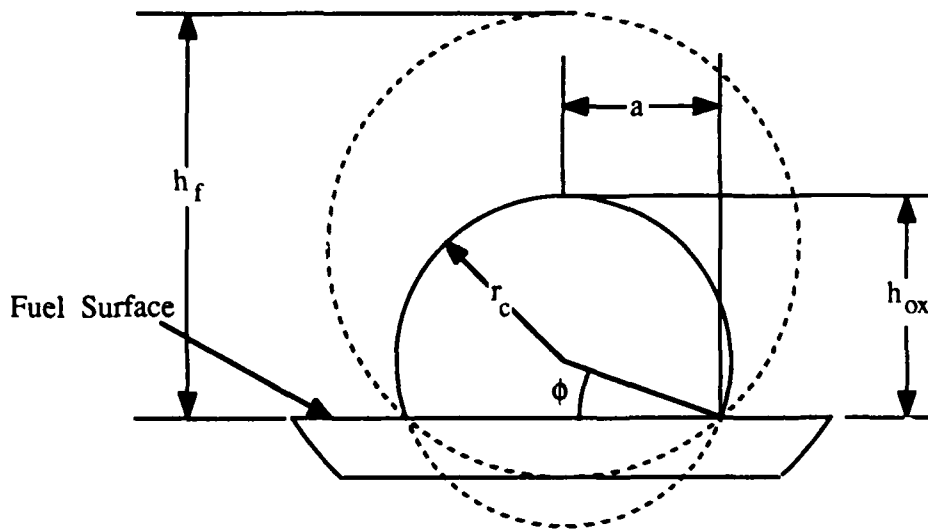

Figure A.12. Radius of Curvature Less than Height Above Surface

The quantity h_{ox} is now the height above the planar fuel surface at which the center of the oxidizer surface will lie. It is obtained by multiplying the time the fuel takes to burn down to height h_f by the burning rate of the oxidizer, and then subtracting this product from the value of h_f. For this case, it can be seen that

$$r_c \sin\phi = h_{ox} - r_c \qquad (A.63)$$

and

$$\cos\phi = \frac{a}{r_c} \qquad (A.64)$$

The results for these equations will be the same as for the concave surface case, with the equation for r_c given by Eq. (A.58) and the equation for the surface area given by Eq. (A.59).

The final possible scenario is where the radius of curvature of the oxidizer surface is greater than h_{ox}, as shown in Fig. A.13.
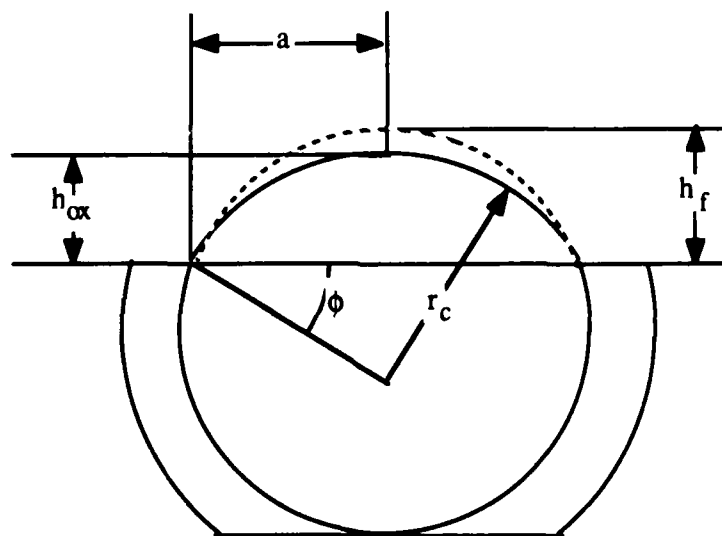

Figure A.13. Radius of Curvature Greater than Height Above Surface

For this case,

$$r_c \sin\phi = r_c - h_{ox} \qquad (A.65)$$

and

$$\cos\phi = \frac{a}{r_c} \qquad (A.66)$$

Once again, Eq. (A.58) can be used to obtain the radius of curvature and Eq. (A.59) can be used to obtain the surface area.

A.5. Calculation of Volumes Consumed.

In order to determine flame temperatures at each iteration step, it is necessary to determine the oxidizer/fuel stoichiometry. In order to determine the stoichiometry, the volume of oxidizer and fuel consumed from one iteration step to the next must be determined.

A.5.1. Calculations Based on Planar Burning Rates.

This is the most straightforward case, and is shown in Fig. A.14.
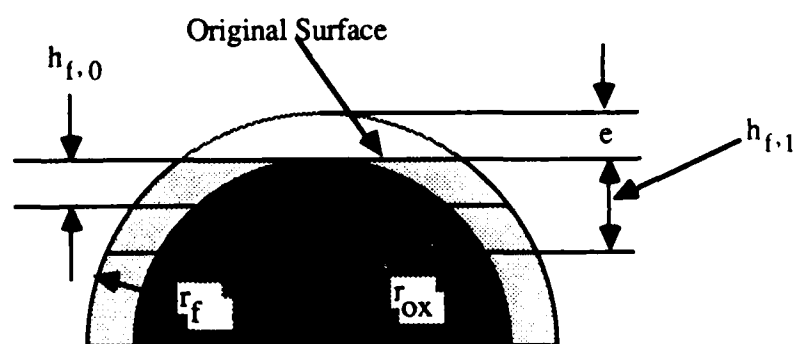
Figure A.14. Calculation of Consumed Volumes Based on Planar Burning

The planar surface's height from the "previous" time step is $h_{f,0}$, and the height from the surface for the current time step is $h_{f,1}$. The volume of oxidizer consumed between increments 0 and 1 is the volume of a spherical cap of radius r_{ox} and height $(h_{f,1} - e)$ minus the volume of a spherical cap of radius r_{ox} and height $(h_{f,0} - e)$. The volume of fuel consumed is the volume of a spherical cap of radius r_f and height $(h_{f,1} + e)$ minus the volume of a spherical cap of radius r_f and height $(h_{f,0} + e)$ and the volume of a

spherical cap of radius r_{ox} and height $h_{f,0}$. The equation for the volume of a spherical cap has been provided as Eq. (A.3).

A.5.2. Calculations With Nonplanar Oxidizer Surface.

The previous method will work for the fuel volume consumed at all times since the fuel surface is always planar. However, the oxidizer surface can be nonplanar, and the calculation of the volume consumed will depend on the geometry of the surface at increments 0 and 1. Four different cases are possible and considered below.

A.5.2.1. Case 1: Surface 0 Convex; Surface 1 Concave.
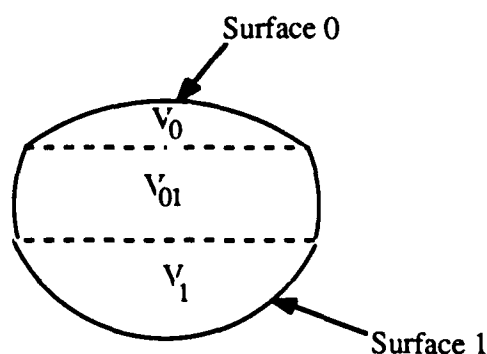
This case is shown in Fig. A.15.

Figure A.15. Surface 1 Convex; Surface 0 Concave

Surface 0 is the surface at the previous time step, and Surface 1 is the surface at the "current" time step. V_0 is the volume of the oxidizer lying above the fuel surface at the previous time step, and V_1 is the volume of the oxidizer lying below the fuel surface at the current time step. V_{01} is the volume of oxidizer contained between the two planar surfaces. V_0 and V_1 can be determined from the equation for a spherical cap, using the values of r_c and h_{ox} for the two respective surfaces; V_{01} is just the volume of oxidizer that would have been consumed if the burning rate had been planar, and can be calculated as described in Sec. A.5.1. So for this case, the total oxidizer consumed is

$$V_{tot} = V_0 + V_1 + V_{01} \qquad \text{(A.67)}$$

A.5.2.2. Case2: Surface 0 Concave; Surface 1 Convex.
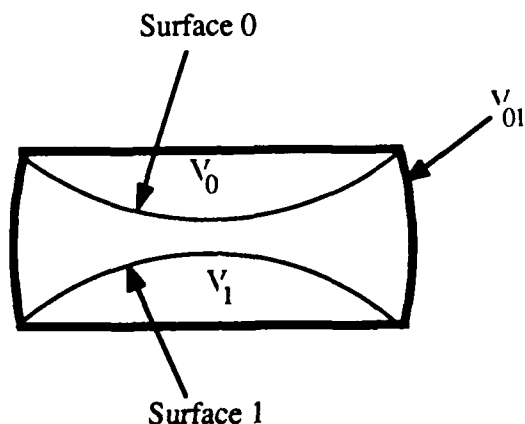
This case is shown in Fig. A.16.

Surface 0

Figure A.16. Surface 0 Concave; Surface 1 Convex

V_{01} is all of the volume contained in the heavy solid outline, and can once again be found by the method of Section A.5.1. V_0 and V_1 can once again be found from the equation of a planar cap using the proper values of r_c and h_{ox}. The total volume consumed is now given by

$$V_{tot} = V_{01} - V_0 - V_1 \qquad \text{(A.68)}$$

A.5.2.3. Case 3: Surface 0 Concave; Surface 1 Concave.

This case is shown in Fig. A.17.

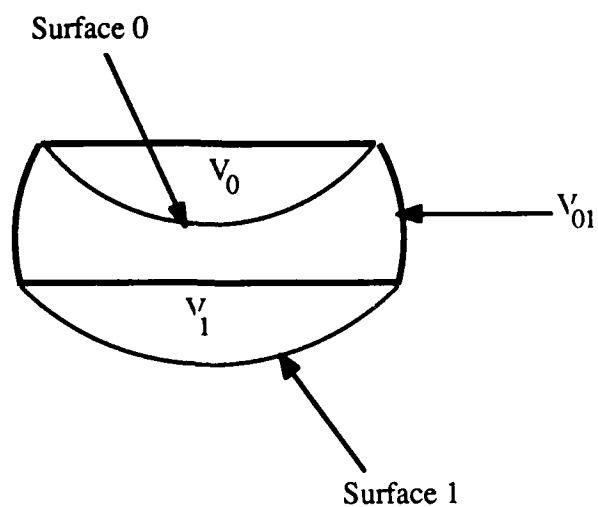Surface 0

V_0

V_{01}'

V_1'

Surface 1

Figure A.17. Surface 0 Concave; Surface 1 Concave

The volume consumed for this case will be equal to

$$V_{tot} = V_1 + V_{01} - V_0 \tag{A.69}$$

A.5.2.4. Case 4: Surface 0 Convex; Surface 1 Convex.

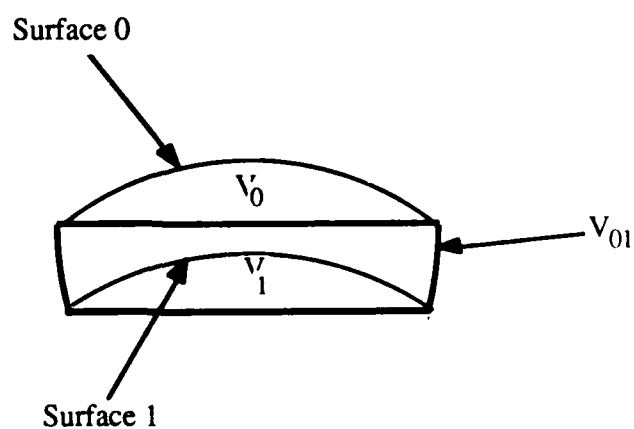This case is shown in Fig. A.18.

Surface 0

V_0'

V_{01}

V_1'

Surface 1

Figure A.18. Surface 0 Convex; Surface 1 Convex

The volume consumed in this case is given by

$$V_{tot} = V_0 + V_{01} - V_1 \qquad (A.70)$$

A.6. Average Surface Diameters and Areas.

It is necessary to determine what the average surface dimameters and areas for the oxidizer and the fuel are between two iteration steps within the COR model. The average areas are needed to determine the average mass flux eminating from the surface between two iterations steps and the diameters of these average areas are used in the Burke-Schuman flame analysis.

A.6.1. Average Oxidizer Diameter Calculation.

Parameters used for this calculation are shown in Fig. A.19.
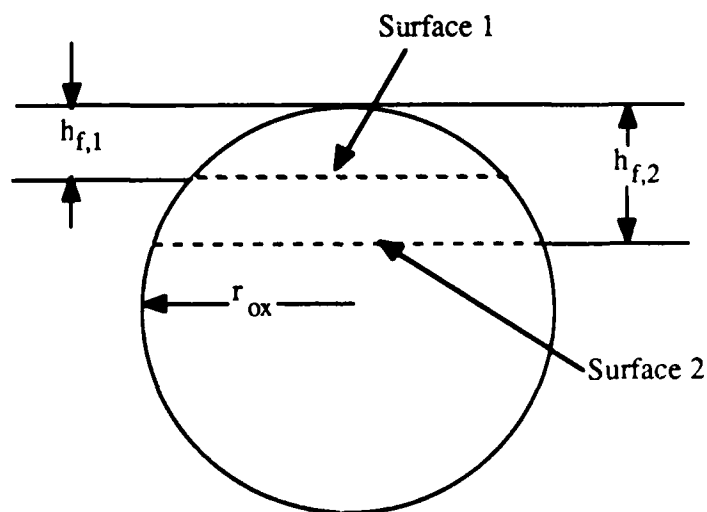

Figure A.19. Parameters for Average Oxidizer Surface Area Calculation

From trigonometry, it can be shown that at any arbitrary height h_f from the surface, the surface radius, which is denoted as a, is given by

$$a = \left[r_{ox}^2 - (r_{ox} - h_f)^2 \right]^{.5}$$
(A.71)

The area of the oxidizer surface at h_f, S_{ox}, is

$$S_{ox} = \pi \, x^2 = \pi \left[r_{ox}^2 - (r_{ox} - h_f)^2 \right]$$
(A.72)

If the dimensionless parameter ξ is defined as h_f/r_{ox} and the dimensionless parameter δ is defined as $S_{ox}/(r_{ox})^2$, δ is given by

$$\delta = \frac{S_{ox}}{r_{ox}^2} = \pi \left[1 - (1-\xi)^2 \right]$$
(A.73)

which simplifies to

$$\delta = \pi \, (2\xi - \xi^2)$$
(A.74)

The average value for δ when the oxidizer burns from the arbitrally selected height $h_{f,1}$ to $h_{f,2}$ needs to be determined. Assuming that the planar fuel surface regresses steadily between these two surfaces, δ_{ave} can be given by

$$\delta_{ave} = (\frac{1}{\xi_2 - \xi_1}) \int_{\xi_1}^{\xi_2} \delta \, d\xi = (\frac{1}{\xi_2 - \xi_1}) \int_{\xi_1}^{\xi_2} (2\xi - \xi^2) \, d\xi \tag{A.75}$$

which, upon integrating, yields,

$$\delta_{ave} = (\frac{\pi}{\xi_2 - \xi_1}) \left[\xi_2^2 - \xi_1^2 - \frac{\xi_2^3}{3} + \frac{\xi_1^3}{3} \right] \tag{A.76}$$

The average oxidzer area $S_{ox(ave)}$ and the average oxidizer diameter $d_{ox(ave)}$ are then given by

$$S_{ox(ave)} = r_{ox} \delta_{ave} \tag{A.77}$$

and

$$d_{ox(ave)} = \frac{D_{ox}}{\sqrt{\pi}} \delta_{ave}^{.5} \tag{A.78}$$

A.6.2. Average Fuel Diameter Calculation.
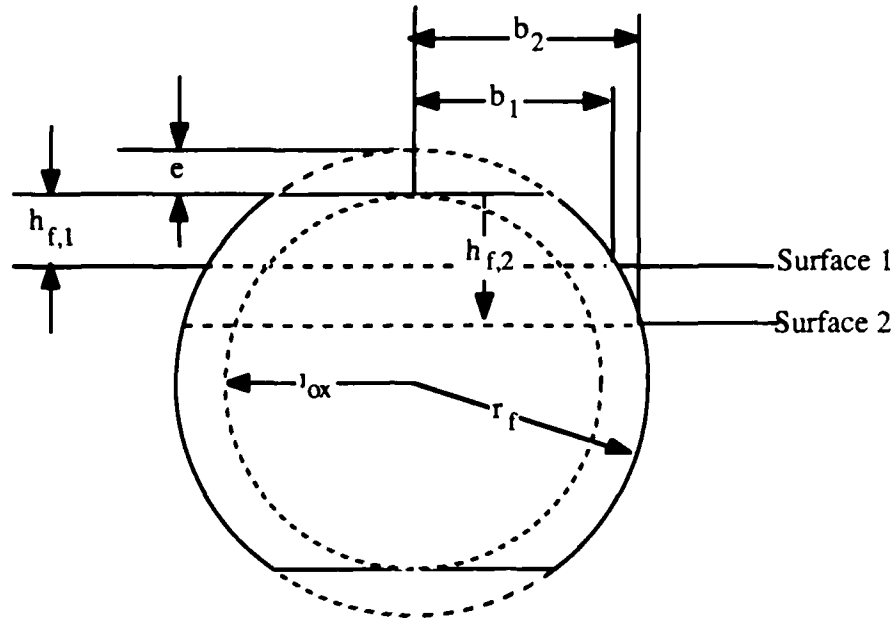
Parameters for this calculation are shown in Fig. A.20.

Figure A.20. Parameters for Average Fuel Diameter Calculation

From trigonometry, it can be shown that the radius of the planar fuel surface, b, can be given by

$$b = \left[r_f^2 - (r_f - h_f - e)^2 \right]^{.5} \tag{A.79}$$

Defining β as b/r_f and ξ' as h_f/r_f, the dimensionless total planar surface area, γ, is given by

$$\gamma = \pi \left[1 - (1 - \xi' - \beta)^2 \right] \tag{A.80}$$

which, upon expanding terms, becomes

$$\gamma = \pi \left[2\xi' + 2\beta - \xi^2 - 2\xi\beta - \beta^2 \right] \tag{A.81}$$

To find the planar surface area of the fuel, the planar surface area of the oxidizer must be subtracted from the total area given in Eq. (A.81). Defining r_{ox}/r_f as η, and δ' as S_{ox}/r_f^2, dividing Eq. (A.72) by r_f results in

$$\delta' = \pi \left[\eta^2 - (\eta - \xi')^2 \right] \qquad (A.82)$$

which, upon simplification, becomes

$$\delta' = \pi \left(2\eta\xi' - \xi'^2 \right) \qquad (A.83)$$

The dimensionless fuel area, σ, is $\gamma - \delta'$, or

$$\sigma = \pi \left[2\xi' + 2\beta - 2\eta\xi - 2\xi\beta - \beta^2 \right] \qquad (A.84)$$

Rearranging terms in Eq. (A.84) yields

$$\sigma = \pi \left[\xi'(2 - 2\eta - 2\beta) + 2\beta - \beta^2 \right] \qquad (A.85)$$

The first set of terms inside the brackets is zero, so the equation reduces to a constant area for the fuel

$$\sigma = \pi \left(2\beta - \beta^2 \right) \qquad (A.86)$$

Substituting for the value of β yields

$$\sigma = \pi \left[2\left(\frac{r_f - r_{ox}}{r_f}\right) - \frac{(r_f - r_{ox})^2}{r_f^2} \right] \tag{A.87}$$

Eq. (A.87) simplifies to

$$S_f = \pi \, (r_f^2 - r_{ox}^2) \tag{A.88}$$

The fuel area is, therefore, a constant value.

To find the fuel diameter corresponding to the average oxidizer diameter, Eq. (A.44) is employed, yielding

$$d_{f(ave)} = \left[D_f^2 - D_{ox}^2 + d_{ox(ave)}^2 \right]^{.5} \tag{A.89}$$

When it is assumed that the fuel is apportioned to the oxidizer at any planar surface in the same proportion as the in the overall propellant, the average fuel diameter can be found from employing Eq. (A.47), yielding

$$d_{f(ave)} = \frac{d_{ox(ave)}}{\sqrt{\zeta_{ox}}} \tag{A.90}$$

Calculation of the average fuel area can then be made from $d_{f(ave)}$.

A.6.3. Average Nonplanar Oxidizer Surface Area.

In calculating a corrected oxidizer mass flux based upon the nonplanar surface of the oxidizer particle, it is necessary to calculate what the average nonplanar area will be between two arbitrary surface intervals. Nomenclature for the average nonplanar oxidizer area calculation is shown in Fig. A.21.
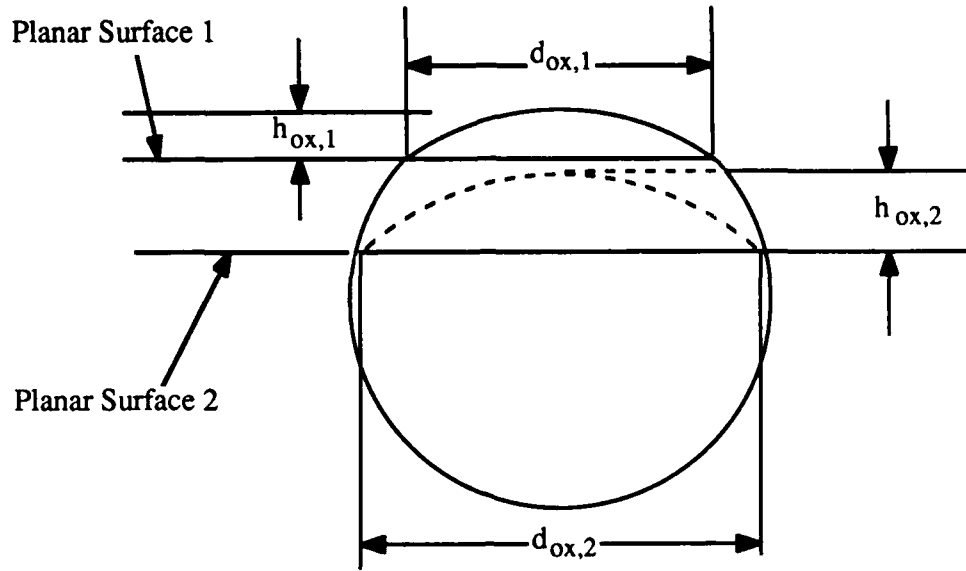
Figure A.21. Nomenclature for Average Nonplanar Oxidizer Surface Area Calculatation

The surface area for the nonplanar oxidizer surface will be the same as that for a conical cap of height h_{ox} and radius of curvature r_c.

$$S_{ox} = 2\pi r_c h_{ox} \qquad (A.91)$$

From Eq. (A.58) the radius of curvature for a surface of height h_{ox} above or below the planar fuel surface must be

$$r_c = \frac{d_{ox}^2}{8h_{ox}} + \frac{h_{ox}}{2} \qquad (A.92)$$

To find the average nonplanar surface area as the value of h_{ox} changes from $h_{ox,1}$ to $h_{ox,2}$, an arithmetic mean, $h_{ox,ave}$ of the two heights is taken. Also, the value of $d_{ox,ave}$, given by Eq. (A.78) is utilized. Using these average values, Eq. (A.91) becomes

$$S_{ox,ave} = \pi \left[\frac{d_{ox,ave}^2}{4} + h_{ox,ave}^2 \right] \qquad (A.93)$$

Substituting for the value of $h_{ox,ave}$ yields

$$S_{ox,ave} = \frac{\pi}{4} \left[d_{ox,ave}^2 + (h_{ox,1} + h_{ox,2})^2 \right] \qquad (A.94)$$

APPENDIX B - HEAT TRANSFER ANALYSIS

In determining of the heat feedback to the surface from any of the possible three flames that can form above the oxidizer particle/fuel binder pair analyzed by this model, the following equation is used to determine the heat flux to a surface from a flame situated above that surface.

$$Q_s = Q_f \exp(-\xi) \qquad \text{(B.1)}$$

In this expression Q_s is the heat transfer to the surface per unit area, Q_f is the heat released per unit area at the flame front, and ξ is a nondimensional height of the flame given by

$$\xi = \frac{x\, m\, c_{p,g}}{\lambda_g} \qquad \text{(B.2)}$$

where x is the height of the flame above the surface, m is the planar burning mass flux from the propellant surface, and $c_{p,g}$ and λ_g are the specific heat and the thermal conductivity of the combustion gases, respectively. This exponential type heat feedback expression can easily be shown to result from an one-dimensional heat transfer analysis of the propellant surface to flame gas phase region.

Equation (B.1) is easily applied to the case of the AP monopropellant flame, since this flame is assumed to be planar being situated at a constant distance above the oxidizer surface. However, both the primary and final diffusion flames have a parabolic shape, and heat transfer to the surface from these flames occurs continuously along the changing height of the flames. For such flames, a modified form of Eq. (B.1) is utilized.

$$Q_s = Q_f \exp(-\varepsilon \xi^*) \qquad \text{(B.3)}$$

In the above expression, the parameter $\varepsilon\xi^*$ is the height from the surface at which a planar flame sheet would have to be located in order to produce the same heat transfer back to the surface that a diffusion flame of maximum height ξ^* would produce. A Burke-Schumann diffusion flame analysis can yield this parameter ξ^*. However, an expression for ε is needed in order to determine the actual heat transfer back to the surface.

According to the Burke-Schumann theory of diffusion flames, a diffusion flame can be one of two different types. The first type of diffusion flame results when the ratio of fuel flow to oxidizer flow within the co-annular jets is greater than the stoichiometic fuel-to-oxidizer mass ratio. In this case, there is an excess of fuel relative to the oxidizer present. In the present analysis of burning oxidizer particles wherein the fuel is issuing from an surrounding annulus, the developing diffusion flame will close over the oxidizer surface. This type of diffusion flame is termed under-ventilated. The second type of diffusion flame results when the ratio of fuel flow to oxidizer flow is less than the stoichiometric fuel-to-oxidizer ratio. In this case, there is an excess of oxidizer present, and the flame will close over the outer fuel surface. This type of diffusion flame is termed over-ventilated. In the following sections, both fully developed and partially developed diffusion flames will be analyzed in order to represent the overall heat transfer from such flames in terms of the parameter $\varepsilon\xi^*$ used in Eq. (B.1) above.

B.1. Fully Developed Diffusion Flames.

B.1.1. Under-ventilated Flames.

For an under-ventilated fully developed diffusion flame, it can be shown that ε is equal to the following. This functional relationship for ε as a function of overall flame height ξ^* has previously been reported by Renie[6].

$$\varepsilon = \frac{1}{\xi^*}\left[\ln(\xi^*\exp(\xi^*)) - \ln(\exp(\xi^*) - 1)\right] \qquad (B.4)$$

B.2.2. Over-ventilated Flames.

The fully developed over-ventilated case, where the flame extends over the fuel binder surface, is represented by Fig. B.1.
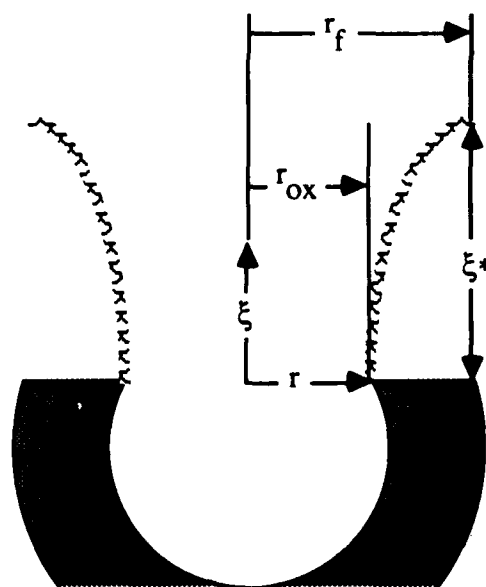

Figure B.1. Over-Ventilated Diffusion Flame

The parameter ξ^* is the maximum height for the diffusion flame above the surface, which occurs at a radial location r_f. The diffusion flame is assumed to be parabolic in shape. For such a flame, the height above the surface at any radial location r can be given by

$$\xi = \xi^* - \frac{r - r_f}{(r_{ox} - r_f)^2} \xi^* \qquad (B.5)$$

The differential heat transfer back to the surface at any location r will be given by

$$dQ_s = Q_f \exp(-\xi) \, r \, dr \, d\theta \qquad (B.6)$$

When the value for ξ in terms of r given by Eq. (B.5) is substituted into Eq. (B.6) the resulting equation is

$$dQ_s = Q_f \exp\left[-\xi*\left(1 - \frac{(r - r_f)^2}{(r_{ox} - r_f)^2}\right)\right] r \, dr \, d\theta \qquad (B.7)$$

Defining a new dimensionless parameter r' as r/r_f, Eq. (B.7) becomes

$$dQ_s = r_f^2 Q_f \exp\left[\xi*\left(\frac{(r' - 1)^2}{((r')_{ox} - 1)^2} - 1\right)\right] r' \, dr' \, d\theta \qquad (B.8)$$

Integrating with the limits on θ from 0 to 2π and on r' from $(r')_{ox}$ to 1, yields the total heat transfer back to the surface in the form

$$Q_s = 2\pi \, r_f^2 \int_{(r')_{ox}}^{1} \exp\left[\xi*\left(\frac{(r' - 1)^2}{((r')_{ox} - 1)^2} - 1\right)\right] r' \, dr' \qquad (B.9)$$

If a planar sheet producing the same amount of heat flux back to the surface as the over-ventilated diffusion flame lies at the height $\varepsilon\xi*$ above the fuel surface, the heat transfer from this flame is

$$Q_s = \pi(r_f^2 - r_{ox}^2) \, Q_f \exp(-\varepsilon\xi*) \qquad (B.10)$$

The heat fluxes of Eqs. (B.9) and (B.10) are equal, so that,

$$\pi \, (r_f^2 - r_{ox}^2) \, Q_f \exp(-\varepsilon\xi^*) = 2\pi \, r_f^2 \int\limits_{(r')_{ox}}^{1} \exp\left[\xi^*\left(\frac{(r'-1)^2}{((r')_{ox}-1)^2} - 1\right)\right] r' \, dr' \qquad (B.11)$$

The integral in Eq. (B.11) must be solved analytically. Designating this integral for the moment as I, Eq. (B.11) can be simplified to

$$\exp(-\varepsilon\xi^*) = \frac{2r_f}{r_f^2 - r_{ox}^2} I \qquad (B.12)$$

Eq. (B.12) can also be expressed as

$$\exp(-\varepsilon\xi^*) = \frac{2}{1 - ((r')_{ox})^2} I \qquad (B.13)$$

The parameter ε can then be found from

$$\varepsilon = \frac{-1}{\xi^*} \ln\left[\frac{2}{1 - ((r')_{ox})^2} I\right] \qquad (B.14)$$

The value for I must still be determined in order to solve for the parameter ε. The procedure used to solve for I was first to select several values of ξ^* at which to solve for ε. For each selected value of ξ^*, a Runge-Kutta scheme was used to solved for I over a range of $(r')_{ox}$ varying from 0.2 to 0.99 (representative of what the range would be as the propellant surface regresses). When I had been solved for over an entire range of $(r')_{ox}$ at a given ξ^*, a second-order curve fit was made for finding I in terms of $(r')_{ox}$. When all of the selected values of ξ^* were solved for in this manner, the coefficients of the second-order curve fits corresponding to each ξ^* were analyzed, and curve fits were produced for relating the second-order coefficients to ξ^*. For values of ξ^* less than 10, a third-order fit of the coefficients was made. For values of ξ^* greater than 10, a logarithmic fit of the coefficents was made.

In the COR model, when the diffusion flame is over-ventilated, the second-order coefficients relating I to $(r')_{ox}$ must first be calculated from the curve fits relating these coefficients to the maximum diffusion flame height ξ^*. Then, when these coefficients are determined, I is computed from the resulting second-order algebraic equation.

B.2. Partially Developed Diffusion Flames.

B.2.1. Under-ventilated Flames.

The case of an under-ventilated primary diffusion flame which is cut off by a planar AP monopropellant flame is shown in Fig. B.2.
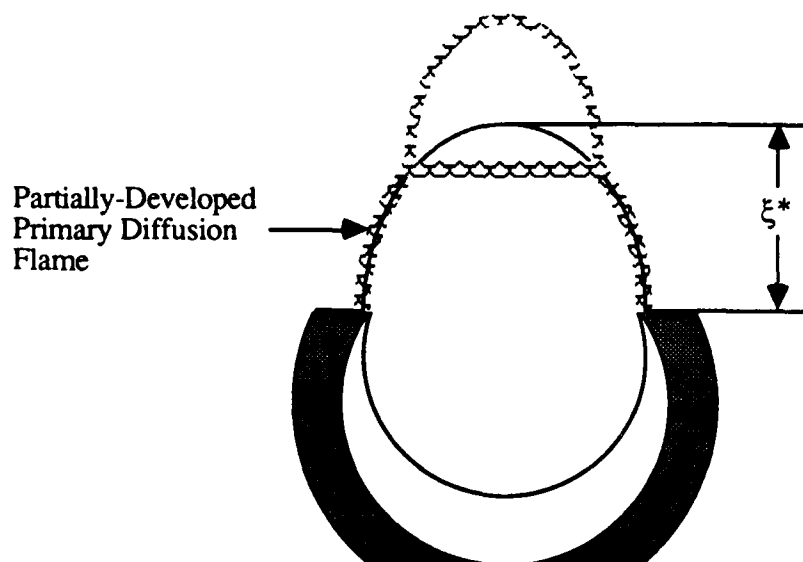

Figure B.2. Partially-Developed Under-Ventilated Diffusion Flame

For this case, it can be shown that the value for ϵ can still be found by Eq. (B.4).

B.2.2. Over-ventilated Flames.

The case for an over-ventilated, partially-developed diffusion flame is shown in Fig. B.3. For this case, r_{PD} is the radius of the primary diffusion flame at the point where the AP monopropellant flame intersects this flame.
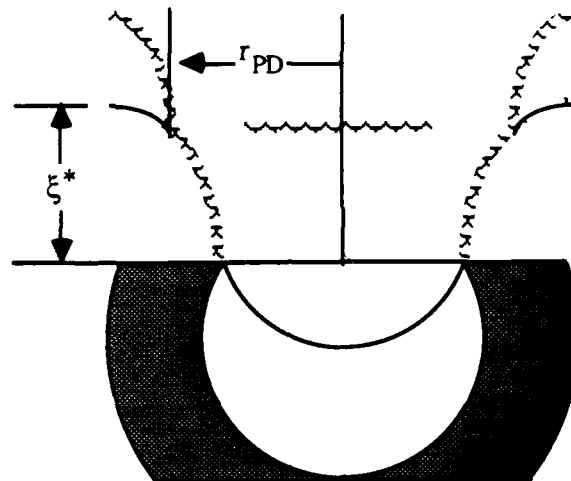

Figure B.3. Partially Developed Over-Ventilated Diffusion Flame

Once again, the diffusion flame is parabolic, and the height of the flame at any radius r can be given by

$$\xi = \xi^* - \frac{(r - r_f)^2}{(r_{ox} - r_f)^2} \xi^* \qquad (B.15)$$

Using the dimensionless paramter r' once again, Eq. (B.15) becomes

$$\xi = \xi^* - \frac{(r' - 1)^2}{((r')_{ox} - 1)^2} \xi^* \qquad (B.16)$$

The total heat transfer from the primary diffusion flame back to the surface will then be given by

$$Q_s = 2\pi\, r_f^2 \int_{(r')_{ox}}^{(r')_{FD}} \exp\left[-\xi * \left(\frac{[r'-1]^2}{[(r')_{ox}-1]^2} - 1\right)\right]\, r'\, dr' \qquad (B.17)$$

The total heat transfer back to the surface can also be expressed as

$$Q_s = 2\pi\, r_f^2 \int_{(r')_{ox}}^{1} \exp\left[\xi * \left(\frac{[r'-1]^2}{[(r')_{ox}-1]^2} - 1\right)\right]\, r'\, dr'$$

$$- 2\pi\, r_f^2 \int_{(r')_{FD}}^{1} \exp\left[\xi * \left(\frac{[r'-1]^2}{[(r')_{ox}-1]^2} - 1\right)\right]\, r'\, dr' \qquad (B.18)$$

To solve Eq. (B.18), the parameter $(r')_{FD}$ must be first determined. From Eq. (C.5) given in the next appendix, it can be seen that

$$(r')_{FD} = 1 - [1 - (r')_{ox}]\sqrt{1 - \frac{x_{AP} - x_{PF}}{x_{PD}}} \qquad (B.19)$$

This value of $(r')_{FD}$ can then be used in Eq. (B.18). The integrals in Eq. (18) can now be solved, as they are the just the negative of the integral I which was evaluated for the case of a fully developed over-ventilated flame. The value for ϵ can then be found from

$$\epsilon = \frac{-1}{\xi *}\left[\ln\left[\frac{2\, I((r')_{ox})}{1 - [(r')_{ox}]^2}\right] - \ln\left[\frac{2\, I((r')_{FD})}{1 - [(r')_{ox}]^2}\right] \right] \qquad (B.20)$$

APPENDIX C - β_F CALCULATION

The parameter β_F is the fraction of the available reactants which will react in the primary diffusion flame, when a primary diffusion flame develops.

C.1. Under-ventilated Primary Flame.

For the case of an under-ventilated primary diffusion flame, it can be shown that β_F is equal to

$$\beta_F = \frac{x_{AP} + x_{PF}}{x_{PD}} \tag{C.1}$$

where x_{AP} is the standoff distance of the AP flame, x_{PF} is the primary flame kinetic standoff distance, and x_{PD} is the standoff distance of a fully developed primary diffusion flame.

C.2. Over-ventilated Primary Flame.

The case where the primary flame is over-ventilated is shown in Fig. C.1. Since an excess of oxidizer is available, the limit to how high the diffusion flame will rise is the amount of fuel available. At the point where the AP flame has cut off the diffusion flame, the portion of the fuel lying between radius r_{ox} and radius $(r_{ox} + r_{FD})$ has been consumed in the reaction, where r_{FD} is the radial location where the AP flame cuts off the primary diffusion flame. Since the amount of fuel is the limiting quantity for the reaction, the fraction of reactants which are consumed in the primary flame is the fraction of the fuel available which is consumed by the primary flame

$$\beta_F = \frac{r_{FD}^2 - r_{ox}^2}{r_f^2 - r_{ox}^2} \tag{C.2}$$

The value of r_{FD} is needed in order to solve for β_F.
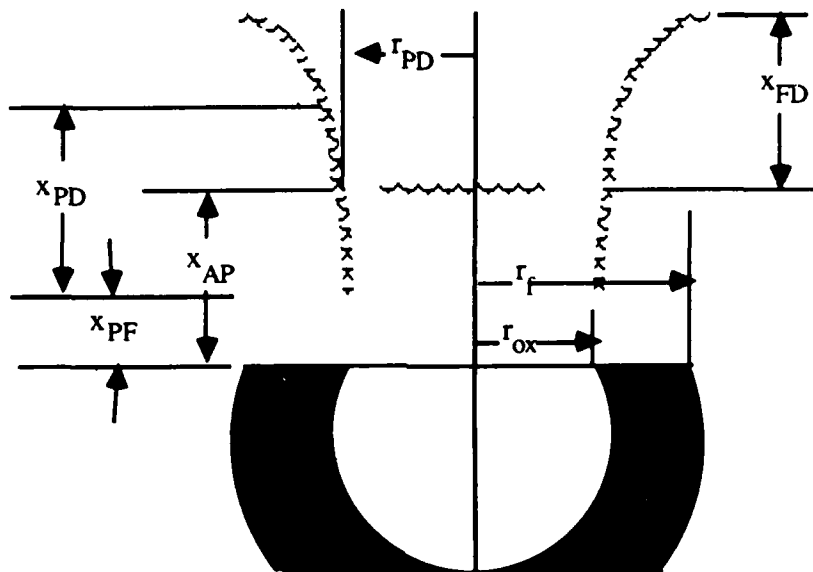

Figure C.1. Over-Ventilated Primary Flame

Since the primary flame is parabolic, the equation relating its height, x, to the radial location r is given by

$$(r - r_f)^2 = \frac{(r_{ox} - r_f)^2}{x_{FD}} (x_{PD} - x) \tag{C.3}$$

The primary flame's height at radial location r_{FD}, relative to the kinetic standoff distance of the primary flame, is $(x_{AP} - x_{PF})$. Substituting this height and r_{FD} into Eq. (C.3) results in

$$(r_{FD} - r_f)^2 = \frac{(r_{ox} - r_f)^2}{x_{PD}} (x_{PD} - x_{AP} + x_{PF}) \qquad (C.4)$$

Solving this equation for r_{FD} results in

$$r_{FD} = r_f - (r_f - r_{ox})\left[1 - \frac{x_{AP} - x_{PF}}{x_{PD}}\right]^{.5} \qquad (C.5)$$

The value for r_{FD} calculated using Eq. (C.5) can then be substituted into Eq. (C.2), and β_F determined.